

**MODELING A DYNAMIC SYSTEM USING FRACTIONAL ORDER
CALCULUS**

by

Jordan Petty

A Thesis

Submitted to the Faculty of Purdue University

In Partial Fulfillment of the Requirements for the degree of

Master of Science



School of Engineering Technology

West Lafayette, Indiana

August 2020

**THE PURDUE UNIVERSITY GRADUATE SCHOOL
STATEMENT OF COMMITTEE APPROVAL**

Dr. Mark French, Chair

School of Engineering Technology

Dr. Jose Garcia Bravo

School of Engineering Technology

Rajarshi Choudhuri

Research Consultant

Approved by:

Dr. Duane Dunlap

*You don't have to be a product of your environment.
Dare to learn and explore, but never forget where you came from.*

ACKNOWLEDGMENTS

First and foremost, I would like to express my appreciation to my fellow research committee members Dr. Richard Mark French, Dr. José Garcia Bravo, and Rajarshi Choudhuri. The following study would not have been accomplished without your support, guidance, and knowledge.

Dr. French, I specifically would like to address your unconditional willingness to help me out from day one of graduate school. I was a graduate student without funding due to unforeseen circumstances, and you presented me the opportunity to join the Technical Assistance Program (TAP) to resolve those conflicts. You have taught me innumerable lessons about engineering and life in general. Furthermore, you and Amy always provided the most warming hospitality imaginable. I can never repay you and Amy for all the baked goodies and feasts throughout my graduate program.

Dad, you have taught me countless lessons about mental fortitude, sacrifice, self-discipline, and work ethic. Mom, you have taught me countless lessons on how to be grateful and appreciate who and what I have. Josh, you have always inspired me to believe in myself, chase down goals, and trust my instincts. Morgan, you have helped me develop emotional intelligence and demonstrated how to be open-minded. Taylor, you have shown me how it is never too late to change the road you are on and make a change for the better. Sylvia, you motivate me to never give up regardless of the challenges ahead. Also, I would like to express my deep love and gratitude to other family members and close friends. Every one of you give me the courage to be what I am destined to be. Without out all of you, I am an unfinished puzzle.

Lastly, I would like to send out appreciation for a few other individuals involved and highlight specific moments throughout my research. Dan Pickett and Dad, I could never repay you for your expertise in CNC machining and willingness to help me during stressful times when I have limited resources to manufacture components. Devon Pessler, I am indebted to you for all the assistance and helping me stay sane during all-nighters in the lab. Doug and Matt Davis, thank you for providing me with a workspace at odd hours, seemingly endless amounts of tools, and assistance assembling the wooden structure.

TABLE OF CONTENTS

LIST OF TABLES	7
LIST OF FIGURES	8
GLOSSARY	9
ABSTRACT.....	11
CHAPTER 1. INTRODUCTION	12
1.1 Overview.....	12
1.2 Significance.....	12
1.3 Statement of Purpose	13
1.4 Experimental Setup.....	13
1.5 Assumptions.....	14
1.6 Limitations	14
1.7 Delimitations.....	14
1.8 Chapter Summary	15
CHAPTER 2. REVIEW OF LITERATURE	16
2.1 Brief History of Fractional Order Calculus	16
2.2 Fractional Order Calculus Explained.....	16
2.2.1 Fractional Derivative of Exponential Functions.....	16
2.2.2 Fractional Derivative of Trigonometric Functions	17
2.2.3 Fractional Derivative of Polynomial Functions.....	18
2.2.4 Fractional Integrals	18
2.2.5 Solving Fractional Order Differential Equations.....	20
2.3 Dynamics	21
2.3.1 Spring-damped System.....	21
2.3.2 Underdamped.....	23
2.4 Fluid Mechanics of the Rotating Disk	24
2.4.1 Boundary Layer Conditions.....	24
2.5 Seminal Theoretical Proposal	26
2.6 Applications	28
2.7 Chapter Summary	28

CHAPTER 3. RESEARCH METHODOLOGY	30
3.1 Research Approach and Hypotheses	30
3.2 Theoretical Models	30
3.2.1 Integer Order Model	30
3.2.2 Fractional Order Model	31
3.3 Related Experiment.....	32
3.4 Experimental Setup.....	34
3.5 Data Acquisition	40
3.6 Data Analysis	43
3.7 Threats to Validity	44
CHAPTER 4. RESULTS	45
4.1 Experimental Data	45
4.2 Comparison of Theoretical Models	46
CHAPTER 5. SUMMARY, CONCLUSION, AND RECOMMENDATIONS	53
LIST OF REFERENCES	55
APPENDIX A. EXPERIMENTAL DATA	57
APPENDIX B. MATLAB CODE	92
APPENDIX C. LIST OF EQUATIONS.....	98

LIST OF TABLES

Table 1. Experimental Data.	57
----------------------------------	----

LIST OF FIGURES

Figure 1.1 Ideal experimental setup (Choudhuri & French, 2018).....	13
Figure 2.1 Illustration of the Lebesgue integral and Riemann integral, respectively (Kleinz & Osler, 2000).....	19
Figure 2.2 Ideal mass-spring-damped system (Jones, 2001).....	22
Figure 2.3 Graph of the underdamped system (Mathworks, 2015).....	24
Figure 2.4 Three-dimensional boundary layer formation on the disk (Choudhuri & French, 2018).....	25
Figure 2.5 Plate with surface area A and mass m is connected to a massless spring with a spring constant k (Magin, 2006).....	27
Figure 3.1 The free body diagram of the oscillating disk for the integer order model (Choudhuri & French, 2018).....	31
Figure 3.2 The free body diagram of the oscillating cylinder with initial boundary conditions for the fractional model (Choudhuri & French, 2018).....	32
Figure 3.3 Experimental setup from previous research (Choudhuri & French, 2018).....	33
Figure 3.4 Image of the bottom support.....	35
Figure 3.5 Radial bearing pressed onto the upper end of the shaft.....	35
Figure 3.6 3D model of the bearing plate fixed to the wooden structure.....	37
Figure 3.7 Experimental setup.....	38
Figure 3.8 3D model of the experimental apparatus.....	39
Figure 3.9 Plot of radius (m) vs. time (sec) to verify camera alignment.....	40
Figure 3.10 Tracker software interface.....	41
Figure 3.11 Tracker recording the position of the black dot.....	42
Figure 3.12 Image of the tracer used for Tracker.....	43
Figure 4.1 Graph of the experimental data from MATLAB.....	46
Figure 4.2 Graph of the integer order model approximation.....	48
Figure 4.3 Graph of the fractional order model approximation.....	49
Figure 4.4 Plot for the comparison of local maxima of the experimental data and models.....	50
Figure 4.5 Plot for squared difference between integer model and experimental data.....	51
Figure 4.6 Plot for the squared difference between fractional model and experimental data.....	52

GLOSSARY

Dynamic system	A system that consists of a mass-spring-damper and has a response to a specific input or is in free response (Choudhuri & French, 2018).
Fractional calculus	A mathematical tool that utilizes a fractional order or imaginary number order of a differentiation or integration operator in an expression (Kulish & Lage, 2002).
Homogenous field	A mathematical definition of a space that possess properties that are the same throughout the space, such as, an ideal fluid or gas (Choudhuri & French, 2018).
Mathematical model	A set of equations and axioms that describe a physical behavior under a certain set of constraints (Choudhuri & French, 2018).
Mittag-Leffler Function	A generalized two parameter complex function that is used for solving of fractional order differential equations (Garrappa & Popolizio, 2018).
Navier-Stokes	A general equation that mathematically describes the motion of an object in a homogenous field (Choudhuri & French, 2018).
Riemann-Liouville	A generalized form for evaluating an integral of fractional order (Magin, 2006).

NOMENCLATURE

${}_a D_b^\alpha$	Fractional order derivative of a function from limit a to b of order α	$\tau_{\theta\theta}$	Angular shear stress of the fluid on the cylinder
$\Gamma(x)$	Euler's Gamma function of x	G_3	Three parameter notation for Green's function
$E_{\alpha,\beta}(x)$	Two parameter Mittag-Leffler function of x	t_p	Planck's time = 5.39106×10^{-44} seconds
m	Mass of an object	I	Second moment of area
c	Damping constant	G	Shear modulus (of steel)
k	Spring constant	h	Height (of the disk)
λ	Eigen value	r_{outer}	Outer radius (of the disk)
ζ	Damping ratio	r_{inner}	Inner radius (of the disk)
ω	Frequency	D_{spring}	Diameter of the torsional spring
ω_n	Natural frequency	L_{spring}	Length of the torsional spring
ω_d	Damped frequency	t	Time (seconds)
ϕ	Phase difference		
Re	Reynolds number		
l_*	Viscous length scale of the disk (top cross section of the cylinder)		
Ω_z	Angular acceleration		
c_f	Skin friction coefficient		
v_τ	Angular shear stress friction velocity		
v_r	Velocity in the radial direction		
v_θ	Velocity in the angular direction		
v_z	Velocity in the vertical (z-axis) direction		
ρ	Density of the material		
μ	Viscosity of the fluid		

ABSTRACT

Fractional calculus is the integration and differentiation to an arbitrary or fractional order. The techniques of fractional calculus are not commonly taught in engineering curricula since physical laws are expressed in integer order notation. Dr. Richard Magin (2006) notes how engineers occasionally encounter dynamic systems in which the integer order methods do not properly model the physical characteristics and lead to numerous mathematical operations. In the following study, the application of fractional order calculus to approximate the angular position of the disk oscillating in a Newtonian fluid was experimentally validated. The proposed experimental study was conducted to model the nonlinear response of an oscillating system using fractional order calculus. The integer and fractional order mathematical models solved the differential equation of motion specific to the experiment. The experimental results were compared to the integer order and the fractional order analytical solutions. The fractional order mathematical model in this study approximated the nonlinear response of the designed system by using the Bagley and Torvik fractional derivative. The analytical results of the experiment indicate that either the integer or fractional order methods can be used to approximate the angular position of the disk oscillating in the homogeneous solution. The following research was in collaboration with Dr. Richard Mark French, Dr. Garcia Bravo, and Rajarshi Choudhuri, and the experimental design was derived from the previous experiments conducted in 2018.

CHAPTER 1. INTRODUCTION

1.1 Overview

Newton and Leibniz founded integer order calculus in the seventeenth century by developing a general symbolic and systematic method of analytical operations. Fractional calculus—the integration and differentiation to an arbitrary or fractional order—was conceptualized nearly the same time as integer order calculus (Kulish & Lage, 2002). Fractional calculus techniques are applied in the following experiment to model the nonlinear response of the proposed oscillatory dynamic system. The comparison of the fractional and integer order model data determines if the oscillatory decay of the spring-damped system demonstrates fractional dynamic behavior.

1.2 Significance

The techniques of fractional calculus are not commonly taught in engineering curricula since physical laws are expressed by integer order notation. Engineers, however, encounter situations in which the integer order methods do not properly model the physical characteristics of a dynamic system and lead to numerous mathematical operations (Magin, 2006). Magin (2006) provides an example—derived from the original work of Torvik and Bagley (1984)—where fractional calculus provided an alternative solution for the surface shear stress developed by the transverse motion of a rigid flat plate in a homogeneous fluid. Kulish and Lage (2002) demonstrated how fractional calculus methods yield the same result in one operation as integer order calculus does in three operations. Fractional and integer order methods were applied in the proposed experiment to model the angular position of the disk while oscillating in the homogeneous fluid. The results from the analyses were then compared to the experimental results. The oscillatory decay in the system exhibited fractional behavior since the experimental results match the results obtained from the fractional analysis.

1.3 Statement of Purpose

The problem addressed by the following experimental study is that integer order calculus does not accurately model all the necessary physical characteristics of dynamic systems and produces numerous mathematical operations (Magin, 2006). The purpose of the study was to experimentally validate the fractional order model of the proposed dynamic system by considering the closeness of fit between the fractional and integer order models compared to the experimental data.

1.4 Experimental Setup

The proposed system, derived from previous experiments conducted by Choudhuri and French (2018), was designed as an aluminum disk rotating about the vertical axis of a stainless-steel shaft where both ends were supported by bearings. The upper-support beam fixed the top end of the torsional spring. The bottom of the torsional spring connected to the upper part of the shaft to enable the oscillating motion in the system. The aluminum disk and stainless-steel shaft were joined using a force fit. The bottom end of the shaft was supported by a ball bearing in which was attached to the bottom of the tank containing the homogeneous fluid. Figure 1.1 illustrates the ideal experimental configuration.

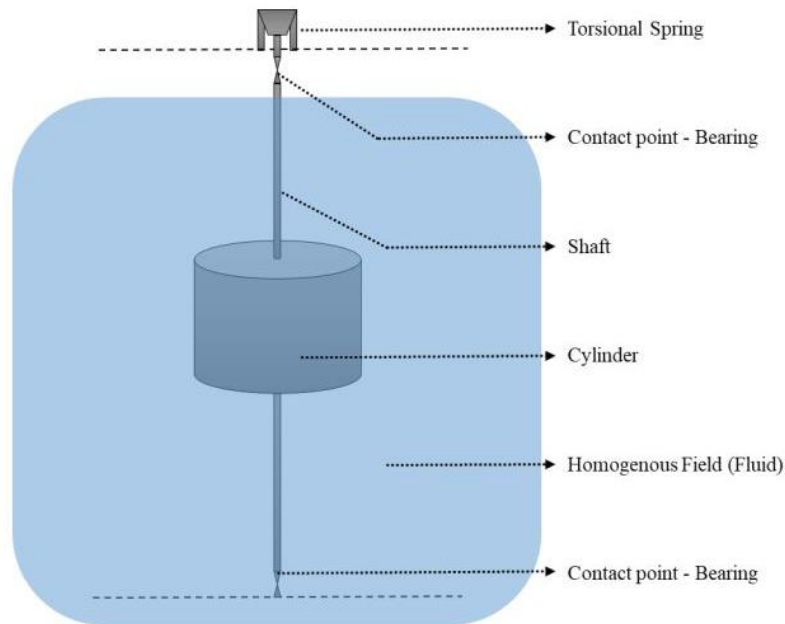


Figure 1.1 Ideal experimental setup (Choudhuri & French, 2018).

1.5 Assumptions

The assumptions of the experiment are listed as follows:

- The boundary conditions at the tank walls do not affect the motion of the disk since the diameter of the tank is significantly larger (at least 3x) than the diameter of the disk.
- Fluid boundary layer effects on the shaft are negligible.
- The surface finish of the disk is uniform meaning that the coefficient of drag is uniform along the surface.
- The contact point between the bottom of the shaft and the bearing fixed to the bottom of the tank is frictionless.
- The homogeneous fluid used in the experiment is considered ideal.

1.6 Limitations

The limitations of the experiment are listed as follows:

- The static and dynamic relationship of the shaft and the disk must remain perpendicular.
- Inertial forces must be high enough, compared to the spring and damping forces, to prevent rapid oscillatory decay.
- The fatigue stresses acting on the torsional spring after each experiment run incurs losses thus the spring must be replaced after each run.

1.7 Delimitations

The delimitations of the experiment are listed as follows:

- Fluid boundary layer formation on the vertical shaft is not considered.
- Variation of the cross-sectional area of the aluminum disk is not considered as it has been machined with tight tolerances and is considered uniform.
- Variation of the surface finish on the top and bottom face of the aluminum disk is not considered as it has been machined with tight tolerances and is considered uniform.

- The alignment of the stainless-steel shaft and aluminum disk is considered perpendicular due to careful machining and tight tolerances.

1.8 Chapter Summary

Newton and Leibniz established the foundations of integer order and fractional order calculus in the seventeenth century. Fractional order calculus is a mathematical concept in which integration and differentiation is to an arbitrary, non-integer order (Kulish & Lage, 2002). The fractional and integer order differential equations corresponding to the experiment were evaluated to model the dynamics of the oscillating system. The purpose of this study was to experimentally validate the application of fractional order calculus to approximate the angular position of the oscillating disk in a homogeneous fluid . The following chapter goes into further details regarding the history, fundamental theories, and applications of fractional order calculus.

CHAPTER 2. REVIEW OF LITERATURE

2.1 Brief History of Fractional Order Calculus

The foundations of calculus emerged during the third century after Archimedes, the father of statics, computed areas, volumes, and lengths of arcs by methods of exhaustion. The method of exhaustion computed the desired area by inscribing polygons in a circle with an increasing number of edges in which the area of the polygons converges to the area of the containing shape (Rosenthal, 1951). Efforts from Stevin, Valerio, Kepler, Cavalieri, Fermat, Pascal, Descartes, and many others set the stage for the two founding fathers of calculus. Newton and Leibniz independently founded integer order calculus by developing a general symbolic and systematic method of analytical operations independent of geometry during the seventeenth century (Rosenthal, 1951). The integer order notation $\frac{df(x)}{dx}$ or $D^1f(x)$, $\frac{d^2f(x)}{dx^2}$ or $D^2f(x)$ is a familiar concept. However, the fractional order notation $\frac{d^{\frac{1}{2}}f(x)}{dx^{\frac{1}{2}}}$ or $D^{\frac{1}{2}}f(x)$ is not easily recognized, because textbooks often do not incorporate lessons on fractional order concepts (Kleinz & Osler, 2000). Fractional calculus—the method of integration and differentiation to an arbitrary, non-integer order—was conceived nearly the same time as integer order calculus in 1695 (Kulish & Lage, 2002). Fractional calculus operations are demonstrated on functions of engineering interest with emphasis on Laplace transform methods to solve initial value problems in the time domain and provide expressions describing sinusoidal steady-state behavior in the following text. In real analyses, fractional order calculus is the generalization of integer order calculus.

2.2 Fractional Order Calculus Explained

2.2.1 Fractional Derivative of Exponential Functions

Kleinz & Osler (2000) provide an explanation of fractional order calculus by examining the exponential function below in equation 2.1.

$$f(x) = e^{px} \quad (2.1)$$

The corresponding integer-based derivative of the first, second, and third order are shown below in equation 2.2.

$$\begin{aligned}
f^1(x) &= D^1 e^{px} = p^1 * e^{px} \\
f^2(x) &= D^2 e^{px} = p^2 * e^{px} \\
f^3(x) &= D^3 e^{px} = p^3 * e^{px}
\end{aligned} \tag{2.2}$$

Assume that n is an integer number and α is a rational number. The general form of the integer derivative of equation 2.2 is shown below in equation 2.3.

$$f^n(x) = D^n e^{px} = p^n * e^{px} \tag{2.3}$$

Substitute α (the rational number) where n (the integer number) appears from equation 2.3 to create equation 2.4 shown below.

$$f^\alpha(x) = D^\alpha e^{px} = p^\alpha * e^{px} \tag{2.4}$$

D^α represents any value for α —integer, rational, irrational, or complex. For example, replace α with the rational number $\frac{1}{2}$ resulting in the $\frac{1}{2}$ order derivative of the exponential function as shown below in equation 2.5.

$$f^{\frac{1}{2}}(x) = D^{\frac{1}{2}} e^{px} = \sqrt{p} * e^{px} \tag{2.5}$$

A positive real α represents a derivative of the function and a negative α represents an integral of the function for the example above (Klein & Osler, 2000). Note, fractional order derivatives use previous information to converge to the solution; whereas, integer order derivatives are defined completely at a point.

2.2.2 Fractional Derivative of Trigonometric Functions

Choudhuri and French (2018) derive the general form of the fractional order derivative of trigonometric functions sine and cosine using Euler's expression shown below in equation 2.6.

$$e^{jx} = \cos(x) + j * \sin(x) \tag{2.6}$$

Substitute equation 2.6 into equation 2.1 to obtain the general form of the fractional order derivative of a trigonometric function shown below as equation 2.7.

$$D^\alpha * e^{jx} = j^\alpha * e^{jx} = e^{j\left(x + \frac{\pi\alpha}{2}\right)} = \cos\left(x + \frac{\pi\alpha}{2}\right) + j * \sin\left(x + \frac{\pi\alpha}{2}\right) \tag{2.7}$$

2.2.3 Fractional Derivative of Polynomial Functions

Kleinz and Osler (2000) provide the generalized derivative of a polynomial in equation 2.8 below.

$$D^n x^p = \frac{p(p-1)(p-2)\dots(p-n+1)(p-n)(p-n-1)\dots 1}{(p-n)(p-n-1)\dots 1} x^{p-n} = \frac{p!}{(p-n)!} x^{p-n} \quad (2.8)$$

Equation 2.8 is the integer expression for $D^n x^p$ and to replace the positive integer n by the arbitrary number α , the gamma function must be used. The gamma function, introduced by Euler in the 18th century, provides meaning to $p!$ and $(p-n)!$ when p and n are not integers. The gamma function represented by equation 2.9 satisfies the property shown below in equation 2.10 (Podlubny, 1999).

$$\Gamma(x) = \int_0^{\infty} e^{-t} t^{x-1} dt \quad (2.9)$$

$$\Gamma(x+1) = x\Gamma(x) \quad (2.10)$$

Equation 2.8 is then rewritten in the following form since integer n is replaced by the non-natural number α as shown in equation 2.11 below.

$$D^\alpha x^p = \frac{\Gamma(p+1)}{\Gamma(p-\alpha+1)} x^{p-\alpha} \quad (2.11)$$

The concept of fractional derivatives is extended to cover a variety of functions by using a Taylor series in terms of x shown below in equation 2.12.

$$f(x) = \sum_{n=0}^{\infty} a_n x^n \quad (2.12)$$

Differentiate equation 2.12 term by term resulting in equation 2.13 shown below.

$$D^\alpha f(x) = \sum_{n=0}^{\infty} a_n D^\alpha x^n = \sum_{n=0}^{\infty} a_n \frac{\Gamma(n+1)}{\Gamma(n-\alpha+1)} x^{n-\alpha} \quad (2.13)$$

Equation 2.13 is the generalized definition of the fractional derivative (Kleinz & Osler, 2000).

2.2.4 Fractional Integrals

Kleinz and Osler (2000) provide the first and second definite integer order integral of a function as shown in equation 2.14 and equation 2.15 below.

$$D^{-1}f(x) = \int_0^x f(t)dt \quad (2.14)$$

$$D^{-2}f(x) = \int_0^x \int_0^{t_2} f(t_1) dt_1 dt_2 \quad (2.15)$$

The left-hand plot found in Figure 2 illustrates the area of integration represented by equation 2.15 from above. The right-hand plot found in Figure 2.1 illustrates how the area of

integration has changed direction after rearranging the order of integration as shown below in equation 2.16.

$$D^{-2}f(x) = \int_0^x \int_{t_1}^x f(t_1) dt_2 dt_1 \quad (2.16)$$

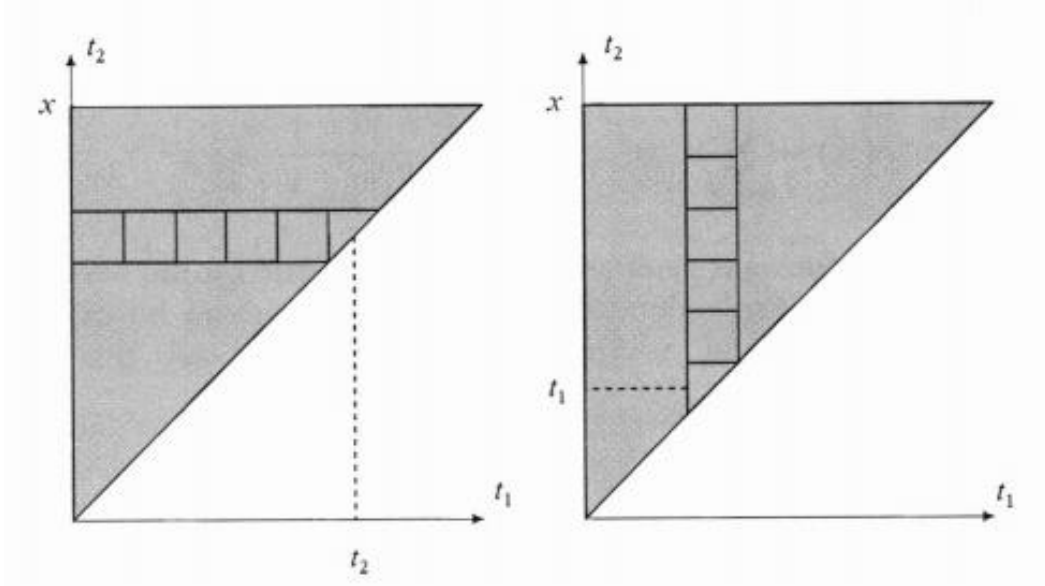


Figure 2.1 Illustration of the Lebesgue integral and Riemann integral, respectively (Klein & Osler, 2000).

Equation 2.16 is changed by moving $f(t_1)$ outside the inner integral since $f(t_1)$ is not a function of t_2 in this example resulting in equation 2.17 shown below.

$$D^{-2}f(x) = \int_0^x f(t)(x - t)dt \quad (2.17)$$

The same procedure is performed for the third and fourth integer-based integrals shown in equation 2.18 and equation 2.19 below.

$$D^{-3}f(x) = \frac{1}{2} \int_0^x f(t)(x - t)^2 dt \quad (2.18)$$

$$D^{-4}f(x) = \frac{1}{2*3} \int_0^x f(t)(x - t)^3 dt \quad (2.19)$$

Considering equations 2.17 to 2.19, the generalized definition of the integer order integral is shown in equation 2.20 below.

$$D^{-n}f(x) = \frac{1}{(n-1)!} \int_0^x f(t)(x - t)^{n-1} dt \quad (2.20)$$

Replace the $-n$ term with the arbitrary α term and the factorial with the gamma function to produce the definition of the Riemann-Liouville fractional order integral. The Riemann-Liouville

fractional integral expression shown below in equation 2.21 is derived from the Laplace transform methods (Magin, 2006).

$${}_b D_x^a f(x) = \frac{1}{\Gamma(-a)} \int_b^x \frac{f(t) dt}{(x-t)^{a+1}} \quad (2.21)$$

The fractional derivative symbol D^a represents positive and negative values for a . The integral is improper if $a > -1$ because as $t \rightarrow x$, $x - t \rightarrow 0$ causing the integral to diverge for every $a \geq 0$. The improper integral converges whenever $-1 < a < 0$ indicating the a term must be negative. Only negative values for a must be used in the example above to consider equation 2.21 as a definition for the fractional integral which is why limits are included (Kleinz & Osler, 2000). The following section outlines how the limit resolves the inherent contradiction found in the definition of fractional calculus and provides methods for solving fractional order differential equations.

2.2.5 Solving Fractional Order Differential Equations

Integer order integrals are expected to have limits hence fractional order integrals are also expected to have limits. Integer-based derivatives are not governed by limits; however, fractional order derivatives surprisingly must have limits. Why must the limit be included for fractional order derivatives if not included for integer order derivatives? Recall equation 2.4 from above containing the fractional derivative for the exponential function. Substitute the fractional derivative of the exponential function from equation 2.4 into the Taylor Series from equation 2.13 resulting in equation 2.22 shown below (Kleinz & Osler, 2000).

$$D^a e^x = \sum_{n=0}^{\infty} \frac{1}{n!} x^n = \sum_{n=0}^{\infty} \frac{x^{n-a}}{\Gamma(n-a+1)} \quad (2.22)$$

The right side of equation 2.22 from above is equivalent to the Taylor series for e^x only when a is an integer. The case in which a is fractional results in two different functions. The expression for the fractional derivative of the exponential function from equation 2.4 is inconsistent with the expression for the fractional derivative of the power function from equation 2.13 since two different limits are being used (Choudhuri & French, 2018).

Notice the fractional integral for an exponential function in equation 2.23 shown below.

$${}_b D_x^{-1} e^{ax} = \int_b^x e^{ax} dx = \frac{1}{a} e^{ax} - \frac{1}{a} e^{ab} \quad (2.23)$$

The limit is incorporated to satisfy equation 2.23 from above. The term $\frac{1}{a} e^{ab} = 0$ when α is positive and the lower limit b is equal to $-\infty$ represented by equation 2.24 below.

$${}_{-\infty}D_x^a e^{ax} = a^a e^{ax} \quad (2.24)$$

The fractional integral with the lower limit equal to $-\infty$ is referred to as the Weyl fractional derivative as seen in equation 2.24 above. The Weyl fractional derivative equation is derived from the Riemann-Liouville fractional order integral expression hence equation 2.25 below (Choudhuri & French, 2018).

$${}_{-\infty}D_x^a f(x) = \frac{1}{\Gamma(-a)} \int_b^x \frac{f(t) dt}{(x-t)^{a+1}} \quad (2.25)$$

2.3 Dynamics

2.3.1 Spring-damped System

Dynamics is defined as the branch of mechanics concerned with bodies in motion. The following section explains how the equations of motion for a single degree of freedom system govern the dynamics for the experimental apparatus by using the ideal mass-spring-damped system for the example. The single degree of freedom mass-spring-damped system used in the following experiment captures the basic behavior of vibrating structures since all structures have mass and stiffness. Proportional damping closely resembles the behavior of vibrating structures and simplifies the mathematical models used in the experiment. Other damping models exist but add complexity to the mathematical models compared to proportional damping. Replacing the proportional damper with the fractional damper presents the possibility of modeling more complicated dynamic behavior. Figure 2.2 shown below illustrates the ideal mass-spring-damped system.

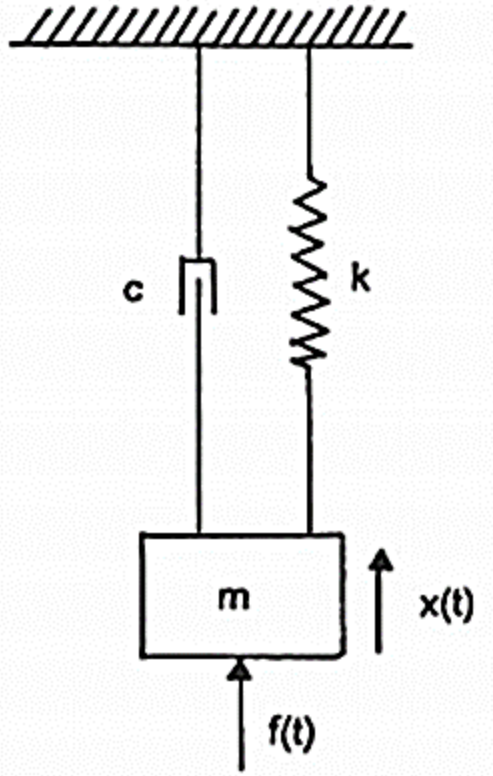


Figure 2.2 Ideal mass-spring-damped system (Jones, 2001).

The equation of motion for the ideal mass-spring-damped system with one degree of freedom is written as:

$$m \frac{d^2x(t)}{dt^2} + c \frac{dx(t)}{dt} + kx(t) = f(t) \quad (2.26)$$

where m is the mass, k is the spring stiffness, and c is the damping coefficient. Equation 2.26 indicates the applied force $f(t)$ is perfectly counteracted by the sum of the inertial force $m \frac{d^2x(t)}{dt^2}$, the stiffness force $c \frac{dx(t)}{dt}$, and the damping force $kx(t)$.

The motion equation from above is rewritten considering the free response characteristic of the system meaning that the external force on the system is equal to zero as shown below in equation 2.27 (Jones, 2001).

$$m \frac{d^2x(t)}{dt^2} + c \frac{dx(t)}{dt} + kx(t) = 0 \quad (2.27)$$

Choudhuri and French (2018) provide the example in which $x(t) = Ae^{\lambda t}$ is the characteristic function hence equation 2.28 and equation 2.29 below.

$$(\lambda^2 m + \lambda c + k)Ae^{\lambda t} = 0 \Rightarrow \lambda^2 m + \lambda c + k = 0 \quad (2.28)$$

$$\lambda_{1,2} = (-\zeta \pm \sqrt{\zeta^2 - 1}) \sqrt{\frac{k}{m}} \quad (2.29)$$

The first and the second order eigenvalues are indicated by $\lambda_{1,2}$ from equation 2.29. Eigenvalues, in context of the proposed experimental study, are numbers that lie on the complex plane and correspond to the roots of the natural frequencies of the system (Howle & Trefethen, 2001). The damping ratio, represented by ζ , is a dimensionless measure describing the oscillatory decay of the system. The expression for the damping ratio is shown in equation 2.30 below.

$$\zeta = \frac{c}{2\sqrt{km}} \quad (2.30)$$

The damping ratio is expressed as a fraction of critical damping. Critically damping indicates that the system returns to equilibrium without oscillating. The experimental apparatus was designed as an underdamped system meaning the oscillatory decay is exponential.

2.3.2 Underdamped

The system is classified as underdamped when the damping ratio is $0 < \zeta < 1$. The roots of the characteristic function from equation 2.28 above are calculated based on the resonant frequency of the system shown in equation 2.31 below:

$$\lambda_{1,2} = -\zeta\omega_n \pm i\omega_d \quad (2.31)$$

where $\omega_n = \sqrt{\frac{k}{m}}$ and $\omega_d = \omega_n\sqrt{1 - \zeta^2}$ for the underdamped case. Figure 2.4 graphically illustrates the underdamped behavior.

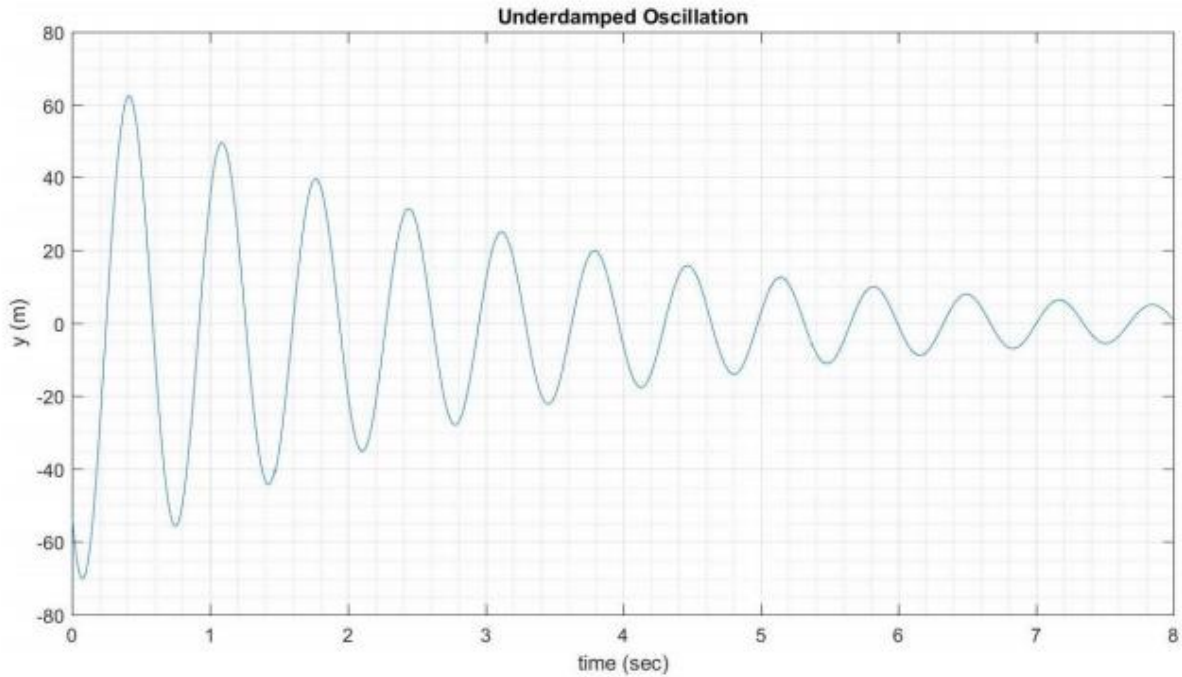


Figure 2.3 Graph of the underdamped system (Mathworks, 2015).

2.4 Fluid Mechanics of the Rotating Disk

2.4.1 Boundary Layer Conditions

The fluid mechanics of the rotating disk are explained in the following section to provide understanding of the boundary layer formation in the proposed experiment. Cham and Head (1969) determined the distribution of the azimuthal and radial velocity field existing within the turbulent boundary layer on a rotating disk as illustrated by Figure 2.4. The red lines model the azimuthal (meaning in the Ω -direction) velocity profiles corresponding to the theoretical laminar flow, the solid black lines model the measured velocity profiles, and the dashed black line models the boundary layer thickness. The azimuthal velocity at the outer part of the boundary layer is less than 20% of the velocity of the disk at the same radius. The measured data starts departing from the theoretical laminar flow model for Reynolds values above $R = 550$ (Imayama, Lingwood, & Alfredsson, 2014).

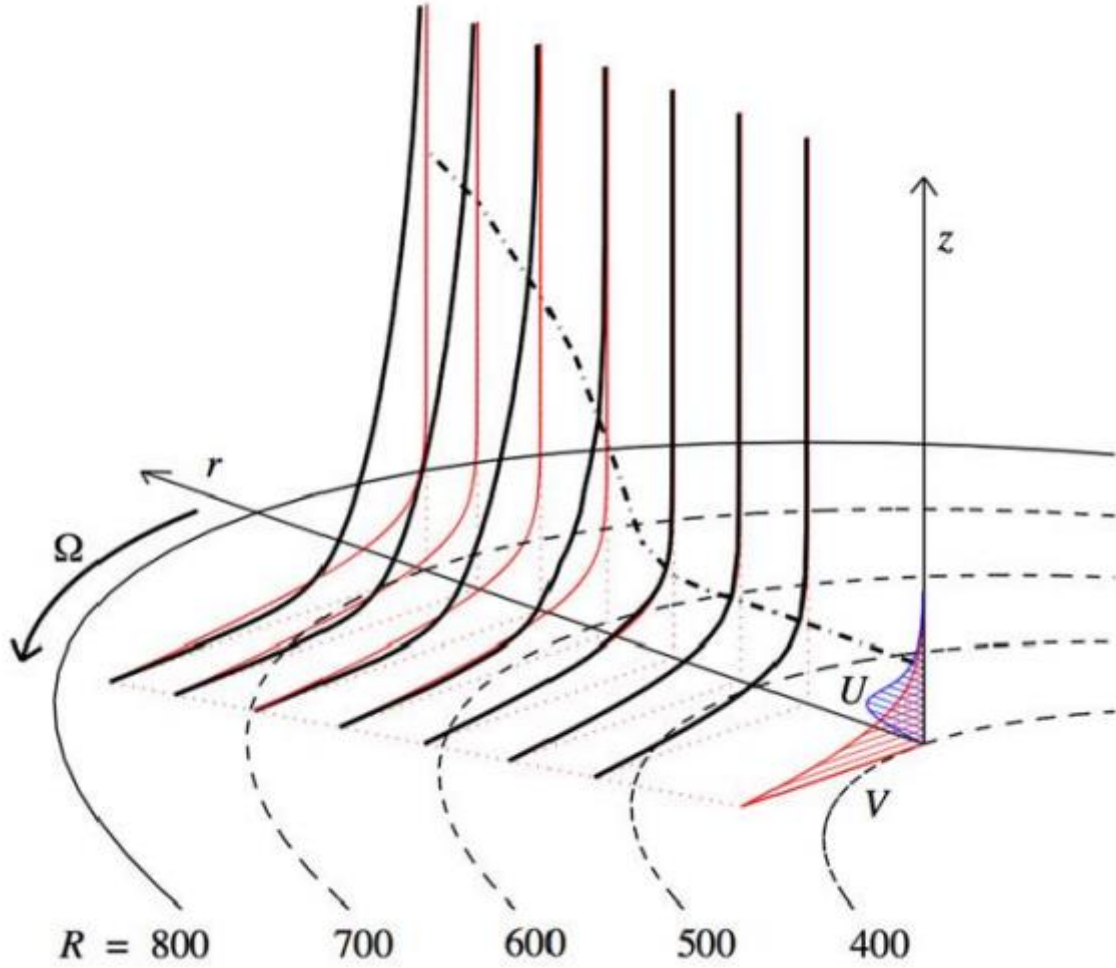


Figure 2.4 Three-dimensional boundary layer formation on the disk (Choudhuri & French, 2018).

The viscous length scale increases proportionately to the radius for a given Reynolds number as shown in the equation below:

$$l_* = \frac{v}{v_\tau} = \frac{v}{\Omega_z r} \sqrt{\frac{2}{c_f}} = Re^{-2} r \sqrt{\frac{2}{c_f}} \quad (2.32)$$

where the friction velocity $v_\tau = \sqrt{\frac{\tau_{\omega,\theta}}{\rho}}$, the wall shear stress in the azimuthal direction $\tau_{\omega,\theta}$, and the fluid density ρ . The skin friction coefficient $c_f = \frac{2v_\tau^2}{(\Omega_z r)^2}$ is a decreasing function of the Reynolds number (Imayama, Lingwood, & Alfredsson, 2014).

The Navier-Stokes differential equation is used to model the flow of incompressible fluids. Choudhuri and French (2018) derived the general form of the Navier-Stokes equation in cylindrical coordinates to obtain the system of fractional order partial differential equations in which model the fluid flow in the proposed experiment as shown in equations 2.33 to 2.35 below.

$$\rho \left(\frac{dv_r}{dt} + v_r \frac{dv_r}{dr} + v_\theta \frac{dv_r}{d\theta} - \frac{v_\theta^2}{r} + v_z \frac{dv_r}{dz} \right) = \rho g_r - \frac{dP}{dr} + \mu \left(\frac{d}{dr} \left(\frac{1}{r} * \frac{d}{dr} (rv_r) \right) + \frac{1}{r^2} * \frac{d^2 v_r}{d\theta^2} - \frac{2}{r^2} * \frac{dv_r}{d\theta} + \frac{d^2 v_r}{dz^2} \right) \quad (2.33)$$

$$\rho \left(\frac{dv_\theta}{dt} + v_r \frac{dv_\theta}{dr} + \frac{v_\theta}{r} * \frac{dv_\theta}{d\theta} + \frac{v_r v_\theta}{r} + v_z \frac{dv_\theta}{dz} \right) = \rho g_\theta - \frac{1}{r} * \frac{dP}{d\theta} + \mu \left(\frac{d}{dr} \left(\frac{1}{r} * \frac{d}{dr} (rv_\theta) \right) + \frac{1}{r^2} * \frac{d^2 v_\theta}{d\theta^2} - \frac{2}{r^2} * \frac{dv_\theta}{d\theta} + \frac{d^2 v_\theta}{dz^2} \right) \quad (2.34)$$

$$\rho \left(\frac{dv_z}{dt} + v_r \frac{dv_z}{dr} + \frac{v_\theta}{r} * \frac{dv_z}{d\theta} + v_z \frac{dv_z}{dz} \right) = \rho g_z - \frac{dP}{dz} + \mu \left(\frac{1}{r} * \frac{d}{dr} \left(r \frac{dv_z}{dr} \right) + \frac{1}{r^2} * \frac{d^2 v_z}{d\theta^2} + \frac{d^2 v_z}{dz^2} \right) \quad (2.35)$$

The continuity equation expresses conservation of mass in the system where the fluid is flowing. The continuity equation and the expression for the shear stress acting on the surface of the disk, shown below as equations 2.36 and 2.37 respectively, are applied to solve the fractional differential equations derived from the Navier-Stokes equation (Choudhuri & French, 2018).

$$\frac{1}{r} * \frac{d}{dr} (rv_r) + \frac{1}{r} * \frac{dv_\theta}{d\theta} + \frac{dv_z}{dz} = 0 \quad (2.36)$$

$$\tau_\theta = -\mu \left[2 \left(\frac{1}{r} * \frac{dv_\theta}{d\theta} + \frac{v_r}{r} \right) - \frac{2}{3} \left(\frac{1}{r} * \frac{d}{dr} (rv_r) + \frac{1}{r} * \frac{v_\theta}{d\theta} + \frac{dv_z}{dz} \right) \right] \quad (2.37)$$

2.5 Seminal Theoretical Proposal

Torvik and Bagley (1984) originally proposed the application of fractional calculus methods to model the oscillating dynamic behavior of the large plate fixed to a massless spring submerged in a homogeneous fluid illustrated in Figure 2.8 below.

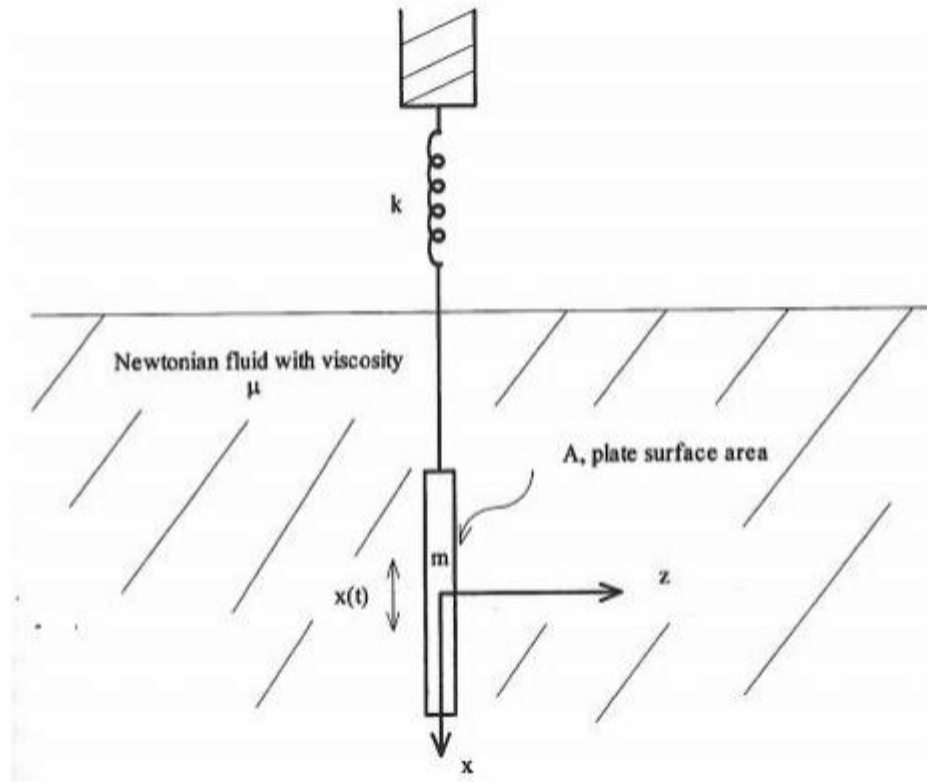


Figure 2.5 Plate with surface area A and mass m is connected to a massless spring with a spring constant k (Magin, 2006).

Oscillatory motion is initiated by the force $f(t)$ applied to the plate in the x -direction. Magin (2006) explains how the application of Newton's second law to the system from Figure 9 yields the following fractional order differential equation:

$$m \frac{d^2 x(t)}{dt^2} + kx(t) + 2A\sqrt{\rho\mu} \frac{d^{\frac{3}{2}} x(t)}{dt^{\frac{3}{2}}} = f(t) \quad (2.38)$$

where m is the mass of the plate, k is the spring constant, A is the surface area of the plate, ρ is the fluid density, μ is the fluid viscosity, and $f(t)$ is the force applied to the plate in the x -direction. The following experiment used the oscillating disk to eliminate leading and trailing edges thus simplifying the mathematical models in comparison to Torvik and Bagley's experiment where a rectangular plate was used.

The general form of Green's function appears in equation 2.39 below (Podlubny, 1999).

$$a {}_0 D_t^\beta y(t) + b {}_0 D_t^\alpha y(t) + c y(t) = f(t) \quad (2.39)$$

The Green's function must be applied to equation 2.39 from above to solve the fractional differential equation with constant coefficients and initial conditions. The analytical solution of equation 2.40 appears below (Podlubny, 1999):

$$y(t) = \int_0^t G_3(t - \tau)f(\tau)d\tau \quad (2.40)$$

where $G_3 = \frac{1}{A} \sum_{k=0}^{\infty} \frac{(-1)^k}{k!} \left(\frac{C}{A}\right)^k t^{2k+1} E_{\frac{1}{2}, 2+\frac{3k}{2}}^k \left(-\frac{B}{A} \sqrt{t}\right)$, $E_{\lambda, \mu}^k = \frac{d^k}{dy^k} E_{\lambda, \mu}(y) = \sum_{j=0}^{\infty} \frac{(j+k)! y^j}{j! \Gamma(\lambda j + \lambda k + \mu)}$,

and $k = 0, 1, 2, \dots$

2.6 Applications

Fractional calculus models a variety of complex dynamic systems more accurately compared to traditional calculus. Recent development for applications of fractional order calculus include but is not limited to fluid mechanics, electrical circuits, heat transfer, signal processing, chemical processes, bioengineering, and automatic control. Torvik and Bagley (1984) experimentally validated the accuracy of the fractional order calculus model by the finite analysis of transient motion in complex viscoelastically-damped structures. The application of fractional calculus to model Proportional Integral Derivative (PID) controllers improved system precision, efficiency, and overall quality of industrial process control compared to the integer order model (Tepljakov, 2017). Ultracapacitors are electrical devices used to store and dissipate energy in applications where a high current is supplied for brief time intervals. The study conducted by Dzieliński, Sarwas, and Sierociuk (2011) revealed how ultracapacitor frequency domain models are intrinsically fractional order. Richard Magin (2006) provides compelling results in which describe the viscoelasticity of human lung tissue using pulmonary impedance models of fractional order.

2.7 Chapter Summary

Fractional calculus—the method of integration and differentiation to an arbitrary, non-integer order—was conceived through combined efforts nearly the same time as integer order calculus in 1695 (Kulish & Lage, 2002). The fractional order notation $\frac{d^{\frac{1}{2}}f(x)}{dx^{\frac{1}{2}}}$ or $D^{\frac{1}{2}}f(x)$ is now familiar considering the fundamental theories and basic operations associated with fractional

calculus methods were explained in detail. Torvik and Bagley (1984) originally proposed the application of fractional calculus methods to model the dynamic behavior of the rectangular plate fixed to a massless spring submerged in a homogeneous fluid. The following experiment incorporated a disk to eliminate the leading and trailing edges thus simplifying the mathematical models. The motivation for the proposed research is derived directly from previous efforts of Choudhuri and French (2018) in which the dynamics of an oscillating cylinder were modeled and experimentally validated to be of fractional order.

CHAPTER 3. RESEARCH METHODOLOGY

3.1 Research Approach and Hypotheses

Can the angular position of a disk oscillating in a homogeneous fluid be calculated using a fractional order mathematical model? Does the fractional order model calculating the angular position of a disk oscillating in a homogeneous fluid yield a more accurate solution than the integer order model? The purpose of this study is to experimentally validate the fractional order model of the proposed dynamic system with a quantitative comparison between the fractional and integer order models.

The margins of error must be considered to make such a comparison for each model. The fractional order model, integer order model, and quantitative comparison to determine the accuracy of each model are the key deliverables of this study. Frictional losses in the bearings, static and dynamic alignment of the components, and rotational forces causing the support structure to flex are key factors affecting the error in the experiment. The hypotheses tested during the experiment are listed as follows:

- **H₀:** The fractional order model of the angular position of the oscillating disk produces less error than the integer order model when comparing the mathematical models to the experimental data.
- **H_a:** The integer order model of the angular position of the oscillating disk produces less error than the fractional order model when comparing the mathematical models to the experimental data.

3.2 Theoretical Models

3.2.1 Integer Order Model

The proposed research compares the integer-based and fractional-based models to determine if the dynamics of the system are of inherent fractional order. The free body diagram for the integer order theoretical model is illustrated by Figure 3.1 below.

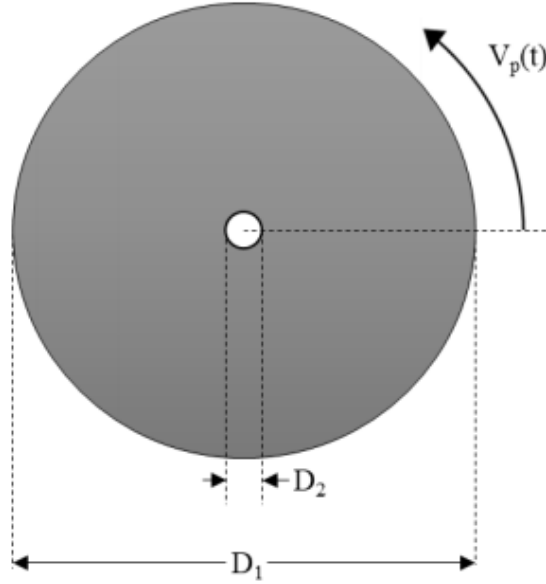


Figure 3.1 The free body diagram of the oscillating disk for the integer order model (Choudhuri & French, 2018).

The integer order equation of motion for the system appears in equation 3.1 below.

$$I \frac{d^2\theta}{dt} + C \frac{d\theta}{dt} + K\theta = f(t) \quad (3.1)$$

The area moment of inertia for the cylinder is calculated using equation 3.2 and the spring constant was calculated using equation 3.3.

$$I = \frac{\pi\rho h}{2} (r_{outer}^4 - r_{inner}^4) \quad (3.2)$$

$$K = \frac{G\pi D_{rod}^4}{32L} \quad (3.3)$$

The general integer order equation for the dynamic system in free oscillation appears in equation 3.2 below:

$$\theta = A \sin(\omega t + \phi) e^{-\sigma t} \quad (3.4)$$

where A is the amplitude, ω is the natural frequency of the system, ϕ is the phase difference, and σ is the shear stress (Choudhuri & French, 2018).

3.2.2 Fractional Order Model

The free body diagram for the fractional theoretical model used in the experiment is illustrated by Figure 3.2 below.

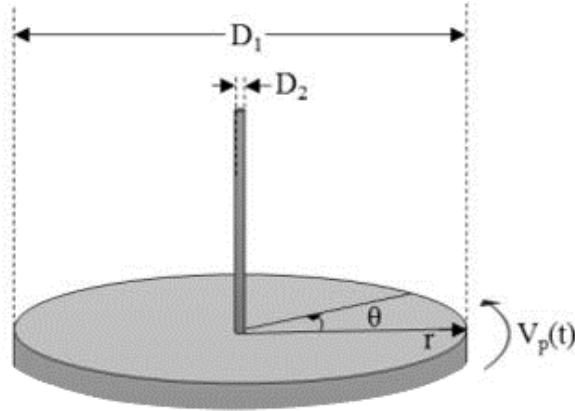


Figure 3.2 The free body diagram of the oscillating cylinder with initial boundary conditions for the fractional model (Choudhuri & French, 2018).

The torsion spring with the spring stiffness K was assumed to be massless and did not cause complications regarding the fluid mechanics of the system. The disk with mass M and area S was assumed to oscillate in the homogeneous fluid with only one degree of freedom. The Bagley-Torvik fractional differential equation was used to compute the numerical solution for the fractional order model as shown in equation 3.3 below:

$$Ay''(t) + B_0 D_t^{3/2} + Cy(t) = f(t) \quad (3.3)$$

$$A = M, \quad B = 2\sqrt{\mu\rho}, \quad C = K$$

where the initial conditions were $y(0) = 18.9132$, $y'(0) = 18.9132$, $f(t) = 0$ (Podlubny, 1999, p. 229). The initial force was zero to simplify the mathematical models approximating the angular position of the oscillating disk.

3.3 Related Experiment

Choudhuri and French (2018) conducted the experimental study of fractional calculus to model the dynamics of a cylinder oscillating while submerged in a homogeneous fluid as illustrated in Figure 2.9 below.

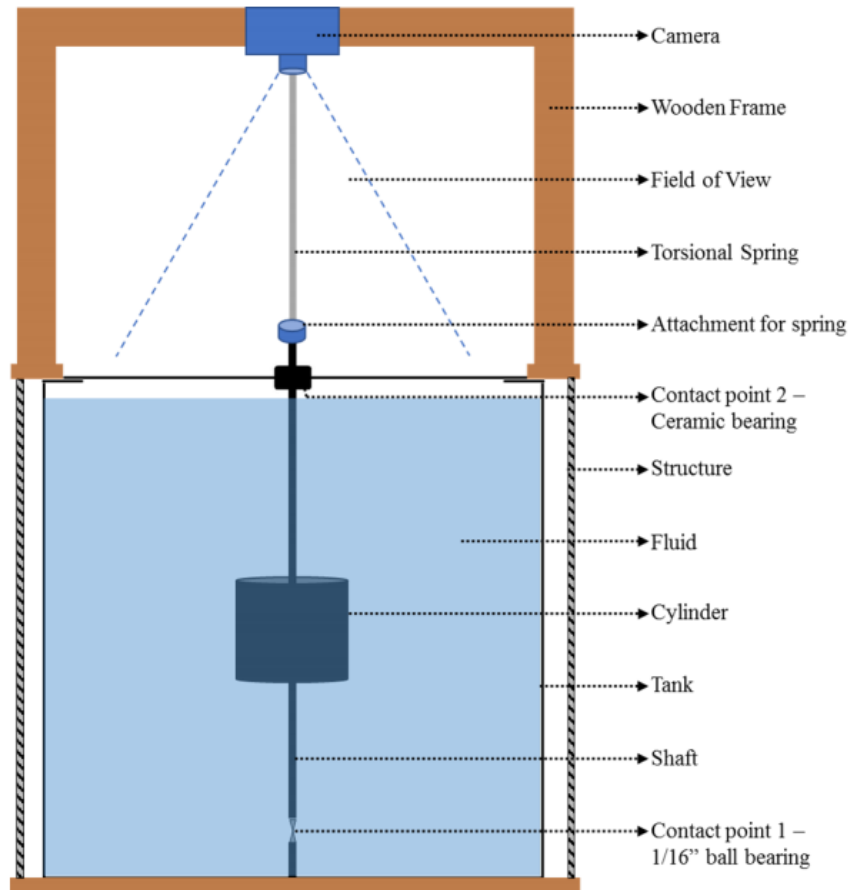


Figure 3.3 Experimental setup from previous research (Choudhuri & French, 2018).

The apparatus illustrated in Figure 3.3 consists of a plastic cylinder made from polyvinyl chloride, an acrylic fish tank, stainless steel shaft, ceramic bearings, steel ball bearing, brazing rod for the spring, camera, and 3D printed material for some of the structural parts. The initial force (spinning force) causes the cylinder to oscillate for 100 seconds before coming to rest again. Testing was conducted in standard temperature and pressure where the cylinder was fully submerged in the homogeneous fluid. The research previously conducted by Choudhuri and French (2018) experimentally validated the fractional order model for the oscillating cylinder submerged in the homogeneous fluid.

3.4 Experimental Setup

The experimental apparatus used in this study was derived from the previous experiment conducted by Choudhuri and French (2018) where an oscillating cylinder was used. The experimental apparatus was designed as an underdamped system to satisfy the general integer order equation of a body in free oscillation found in equation 3.4 above. In this experiment, an aluminum disk was used as the body oscillating in the homogeneous fluid and was made from 6061 aluminum. The aluminum disk was machined to have an outer diameter of 9.817 inches, an inner diameter of 0.4985 inches, and a height of 2.424 inches. The flatness and cylindricity geometric tolerances were controlled while machining the aluminum disk to produce a uniform surface finish. The inner diameter through hole tolerances were controlled to ensure a successful shrink fit between the disk and shaft. The uniform surface finish of the disk produced a uniform drag coefficient along the top and bottom surfaces. The precision ground, polished shaft was purchased from McMaster Carr with a diametral tolerance of -0.0002 inches to 0 inches and a straightness tolerance of 0 inches to 0.0048 inches per foot. The shaft was made from 303 stainless steel with a measured diameter of 0.5000 inches. Micrometers and calipers were used to inspect the dimensions of the machined components. The disk and shaft were joined with a shrink fit, and the disk was carefully positioned at half of the height of the tank which was 12 inches from the bottom of the tank. The tolerances of the components were ideal to minimize fluid layer boundary effects incurring around the shaft and maintain the perpendicular alignment required between the disk and the shaft. The disk oscillated about the vertical axis of the shaft where both ends of the shaft were supported by bearings. A short shaft approximately 2 inches in length was cut from the main section of the shaft and fixed into the base of the apparatus. The base was a 3D printed housing designed for the short section of the shaft which was attached to the bottom of the tank with epoxy. The short shaft and main shaft were coupled by the lubricated 0.25-inch ball bearing. Figure 3.3 is an image of the bottom support where the bottom shaft was coupled to the main shaft with the 0.25-inch ball bearing. The tank used in the experiment had a 36-inch diameter with a 24-inch height.



Figure 3.4 Image of the bottom support.

The upper end of the shaft was machined to allow one end of the music wire to slide inside the pocket. Threaded holes were included for the set screws to fix the end of the wire in place. The radial bearing purchased from Bearing Headquarters Company was pressed onto the upper end of the shaft. Figure 3.4 is an image depicting the radial bearing pressed onto the upper end of the shaft.

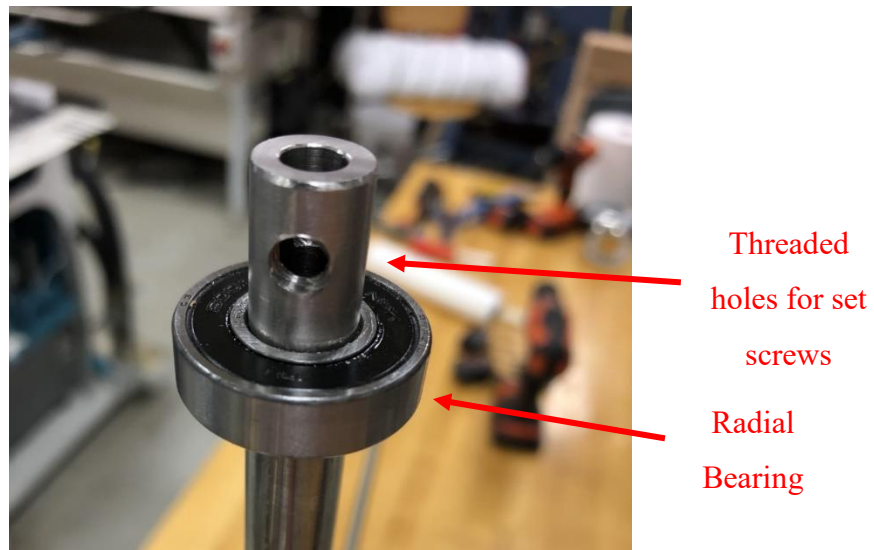


Figure 3.5 Radial bearing pressed onto the upper end of the shaft.

The radial bearing was then press-fitted into a 3D printed plate to support and center the vertical alignment of the shaft. The 3D printed plate was fixed to the wooden frame using screws and wing nuts. Figure 3.6 below contains a screenshot of the 3D model illustrating how the bearing plate was fixed to the wooden frame. The music wire with a measured diameter of 0.21875-inch and a measured length of 28 inches served as the torsional spring. The upper and lower crossbeams of the wooden structure supported the top and bottom ends of the music wire in which both ends were fixed by stainless steel set screws. Figure 3.7 found below contains an image of the experimental setup. Figure 3.8 contains a screenshot of the 3D model of the experimental apparatus.

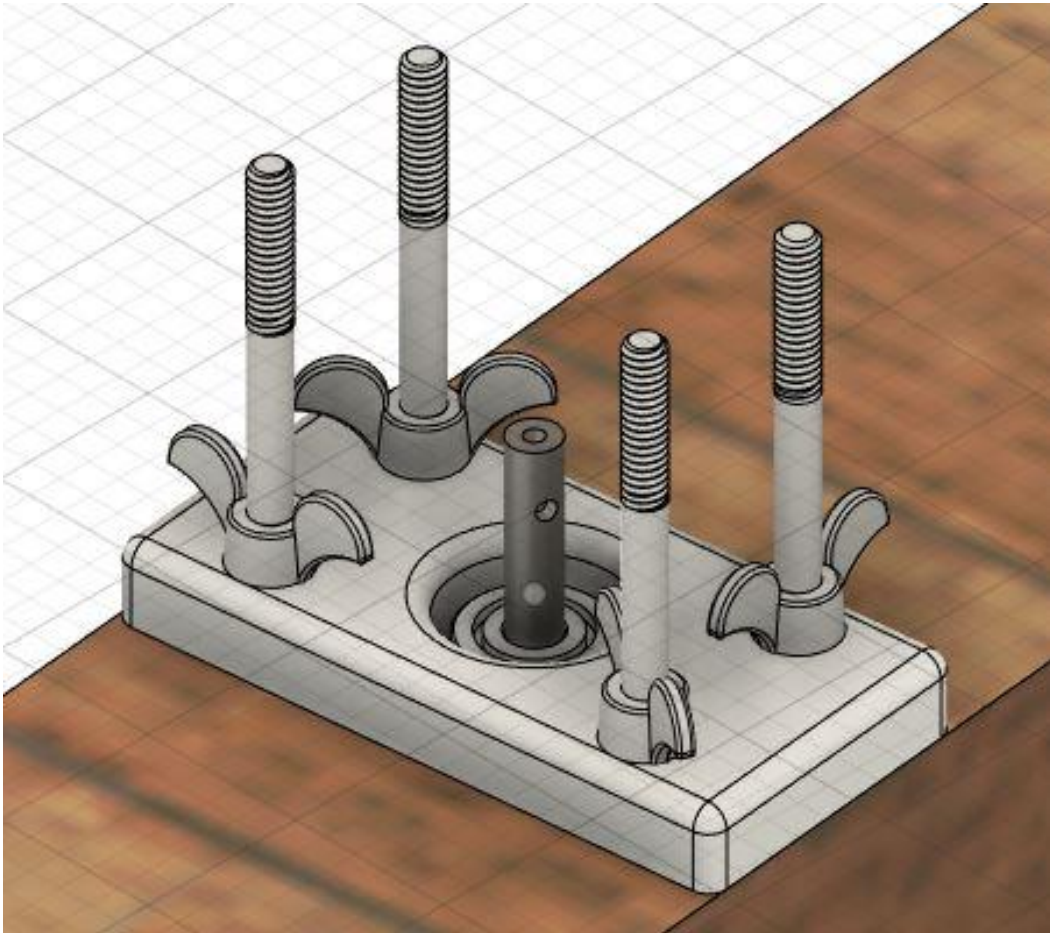


Figure 3.6 3D model of the bearing plate fixed to the wooden structure.

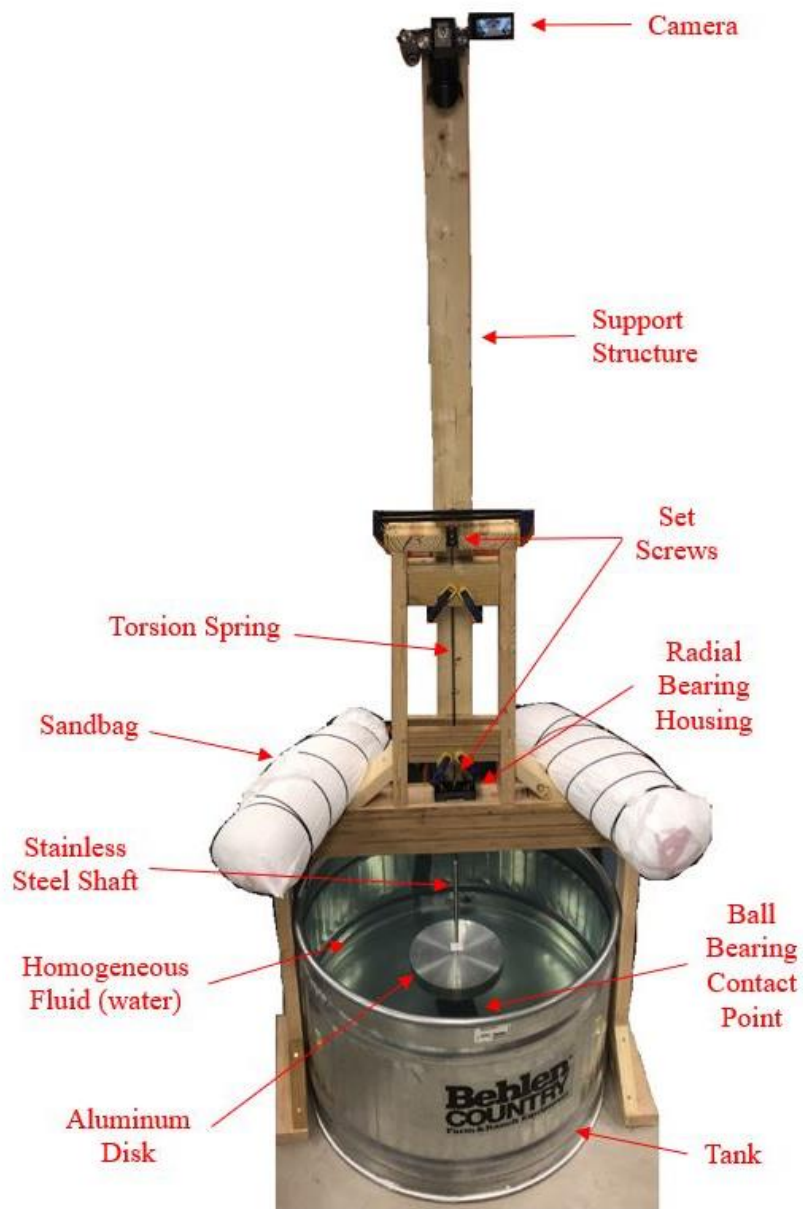


Figure 3.7 Experimental setup.

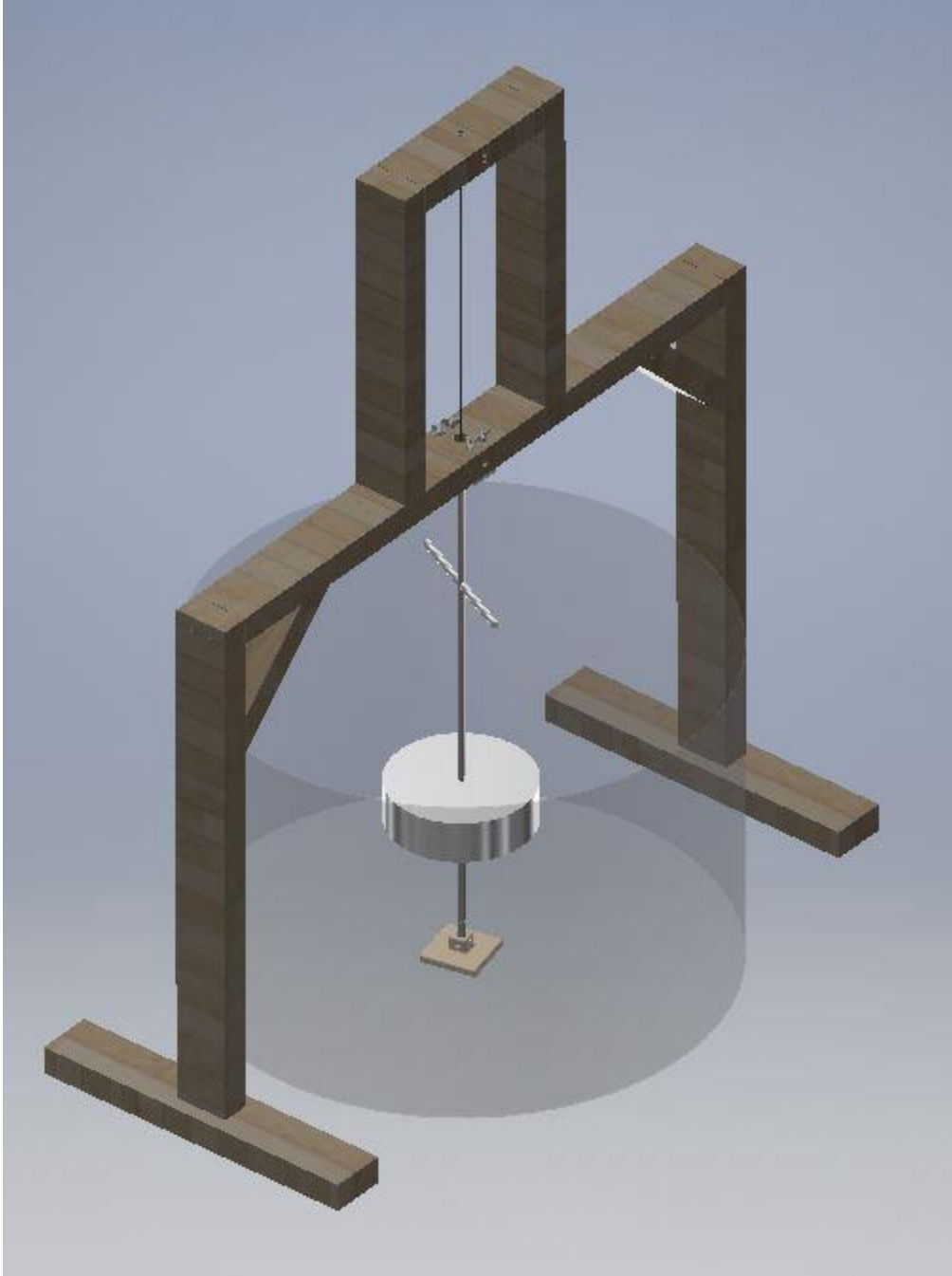


Figure 3.8 3D model of the experimental apparatus.

The center axis of the camera lens was constrained to the vertical axis of the shaft to eliminate parallax. The fully threaded rod supporting the tracer extends 12 inches from the threaded hole through the shaft. The threaded rod extending from the shaft was considered as the radius for calibration purposes. The camera was accurately positioned and calibrated by

collecting data in Tracker and generating a plot of the radius versus time. The plot shown in Figure 3.9 below verified the alignment of the center axis of the camera lens to the vertical axis of the shaft by producing a constant value for radius as a function of time.

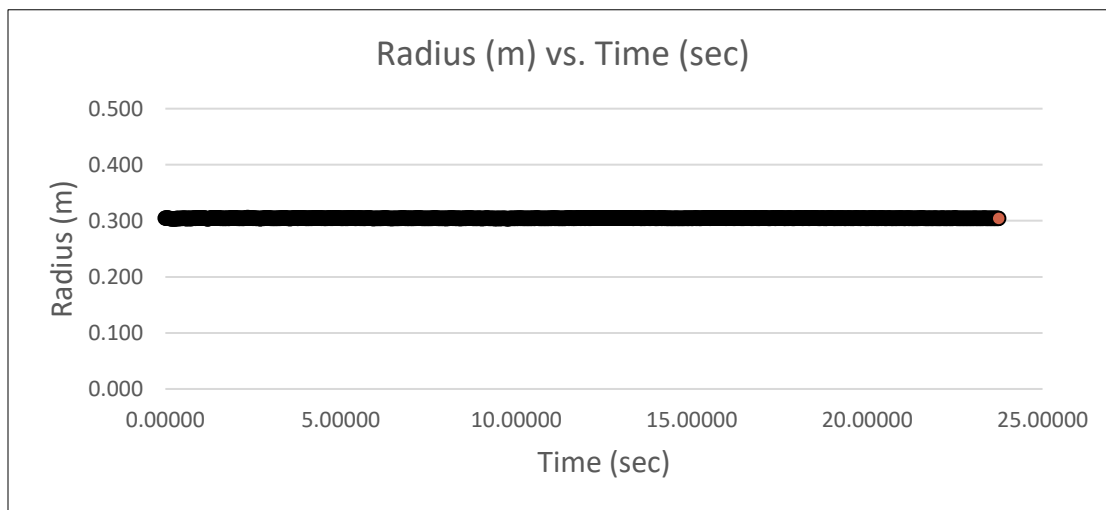


Figure 3.9 Plot of radius (m) vs. time (sec) to verify camera alignment.

3.5 Data Acquisition

The experiment was conducted in an environment with standard temperature and pressure. Video data was acquired using a Panasonic LUMIX G7 camera with specifications of 60 frames per second and shutter speed of 1/1000 seconds. The camera was mounted 9 feet and 9 inches from the ground pointed downward to view into the tank. The MP4 file created from the video recording was uploaded into Tracker—an open source physics software. Figure 3.10 contains a screenshot of the Tracker software interface displaying the camera’s view from above the apparatus.

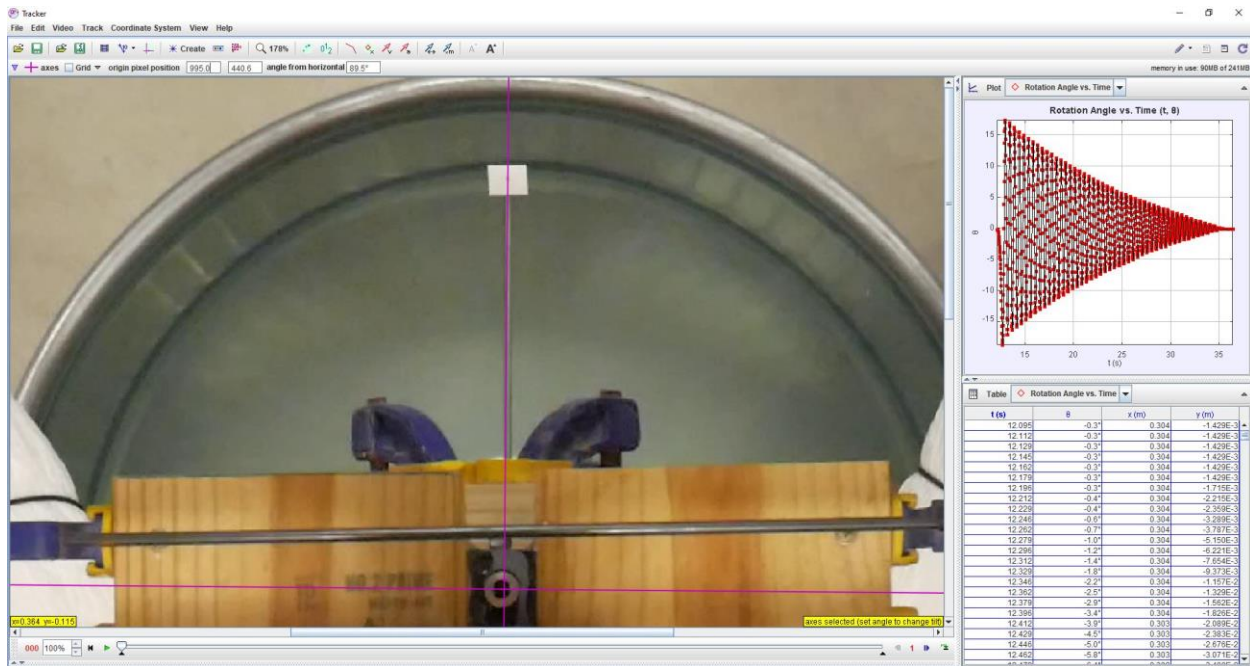


Figure 3.10 Tracker software interface.

Using Tracker, the necessary frames of reference and relative positions for the components were created by following the tracer. The tracer was a rectangular piece of white cardboard fixed onto the end of the threaded rod. The black dot was placed in the center of the white cardboard rectangle allowing the software to accurately track the radial position of the oscillating disk. Figure 3.11 contains a screenshot of Tracker recording the position of the black dot.

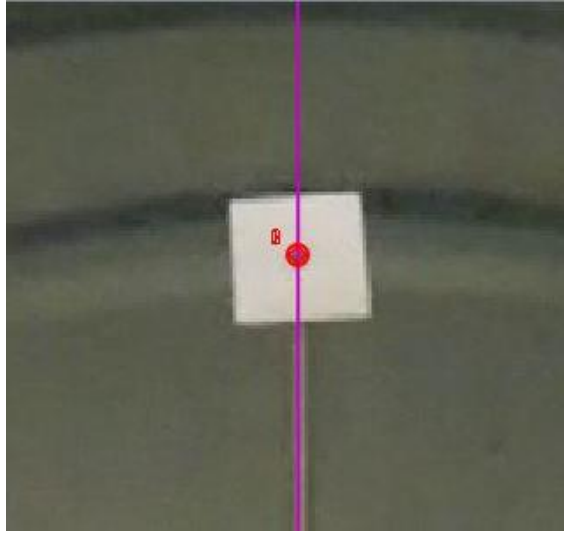


Figure 3.11 Tracker recording the position of the black dot.

The threaded hole was machined into the shaft to mate with a fully threaded rod supporting the tracer. Plumbing tape was included where the fully threaded rod mated with the shaft to damp the vibrations generated while applying the initial spin force. Figure 3.12 contains an image of the fully threaded rod supporting the tracer used during the experiment.



Figure 3.12 Image of the tracer used for Tracker.

3.6 Data Analysis

Tracker software was used to acquire the data and create a text file by exporting to the Notepad application found on the computer. The text file containing the experimental data collected by Tracker was imported to MATLAB using a built-in function and processed to generate the fractional and integer order models. MATLAB produced graphical representations of the integer and fractional order models superimposed on the experimental data plot. The quantitative comparison between graphs determined if the dynamics of the spring-damped oscillating system are considered intrinsically fractional order. The squared difference calculated between the experimental data and the mathematical models was the primary metric to determine error for each model in this study. The more accurate model incurred the least amount of error when compared to the experimental data. Further details regarding error calculations are included in the Results section below.

3.7 Threats to Validity

Mechanical and frictional losses were controlled by proper alignment between components. Tight machining tolerances were maintained throughout the development of the experimental apparatus to ensure perpendicularity between the stainless steel shaft and the aluminum disk. Uneven loading because of misalignment between the aluminum disk and stainless steel introduces frictional forces to the system. The system is assumed to be in free response meaning at $t = 0$ seconds the input force is $f(t) = 0$. Although the system is assumed to be in free response, the input spin force needed to initiate oscillation potentially introduces uneven loading considering the input spin force is performed by hand motion. Proper alignment of the components was also verified by using a level to ensure the ground was not sloped where the apparatus was placed. Additionally, the bottom of the tank was inspected to ensure that the 3D-printed bottom support was level. The torsion spring was replaced every trial to eliminate mechanical losses caused by rotational fatigue stress and to minimize variation in the spring stiffness since the mathematical models use constant coefficients to approximate the angular position of the oscillating disk. Rotational angles of 30 degrees or larger resulted in plastic deformation of the torsion spring, and the wooden support structure flexed while the angles of rotation exceeded 30 degrees. The center axis of the camera lens was constrained to the vertical axis of the stainless steel shaft to minimize parallax and a plot of radius versus time was created to calibrate the camera position as seen in Figure 3.9 above. Quality inspections of component dimensions were accomplished using measurement equipment such as micrometers and calipers. All components of the experimental apparatus were visually inspected for defects before use.

CHAPTER 4. RESULTS

4.1 Experimental Data

The experimental apparatus was designed to be an underdamped system; however, the oscillatory decay does not perfectly mimic exponential decay. The input spin force is performed by hand motion and suspected to cause uneven loading resulting in frictional loss until the system balances and is in free response oscillation. The fatigue stresses acting on the torsion spring are suspected to cause plastic deformation after 30-40 oscillations and are suspected to be the source of difference after $t = 15$ seconds. The following sections explain further details regarding the discrepancies of the data and elaborate on the quantitative comparison between the mathematical models and the experimental data. The experimental data is graphically represented in Figure 4.1 below and the table containing the experimental data is in Appendix A located at the end of the document.

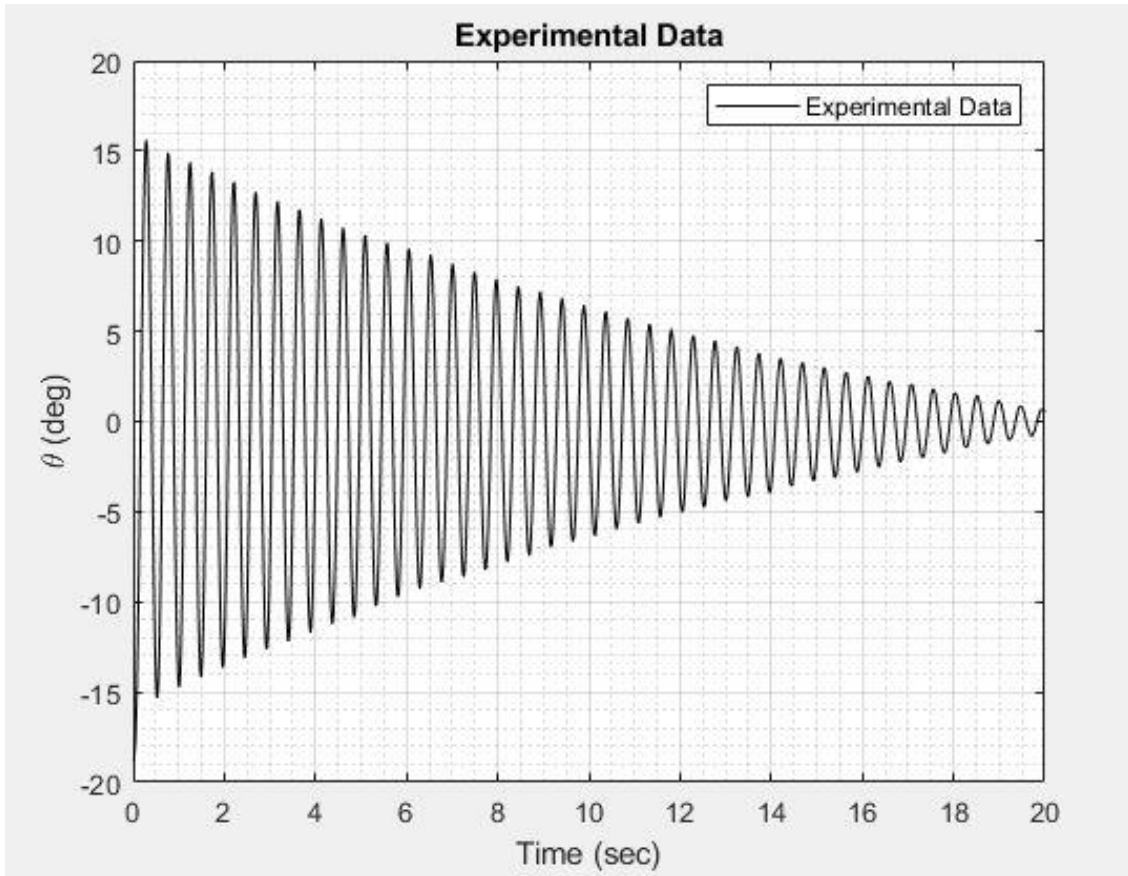


Figure 4.1 Graph of the experimental data from MATLAB.

4.2 Comparison of Theoretical Models

The integer and fractional order models were computed using finite difference approximation methods which are used to find numerical solutions of differential equations. Figure 4.2 and Figure 4.3 are graphical representations of the integer and fractional order models, respectively. Figure 4.4 graphically compares the local maxima of the experimental data and integer and fractional order models.

The local maxima for each was calculated using the built-in MATLAB function named `findpeaks` which returns a vector with the local maxima of the input signal. Figure 4.5 and Figure 4.6 graphically illustrates the squared difference between the integer model versus the experimental data and the fractional model versus the experimental data, respectively. Equation 4.1 below represents how the squared difference was calculated for the quantitative comparison between the models and experimental data.

$$\text{Squared Difference} = (\theta_{calc} - \theta_{exp})^2 \quad (4.1)$$

Referring to Figure 4.5 and Figure 4.6, the largest squared difference calculated was 7.77 degrees squared between the integer order model and the experimental data and 7.849 degrees squared between the fractional order model and the experimental data. The largest squared difference occurred at $t = 0$ seconds. The input spin force is performed by hand motion and suspected to cause uneven loading resulting in frictional loss until the system balances and is in free response oscillation. The squared difference between the mathematical models and the experimental data approaches zero from $t = 5$ seconds to $t = 15$ seconds. After $t = 15$ seconds, the largest squared difference calculated between the experimental data and the integer and fractional models is 2.00 degrees squared and 1.50 degrees squared, respectively. The fatigue stresses acting on the torsion spring are suspected to cause plastic deformation after 30-40 oscillations and are suspected to be the source of difference after $t = 15$ seconds.

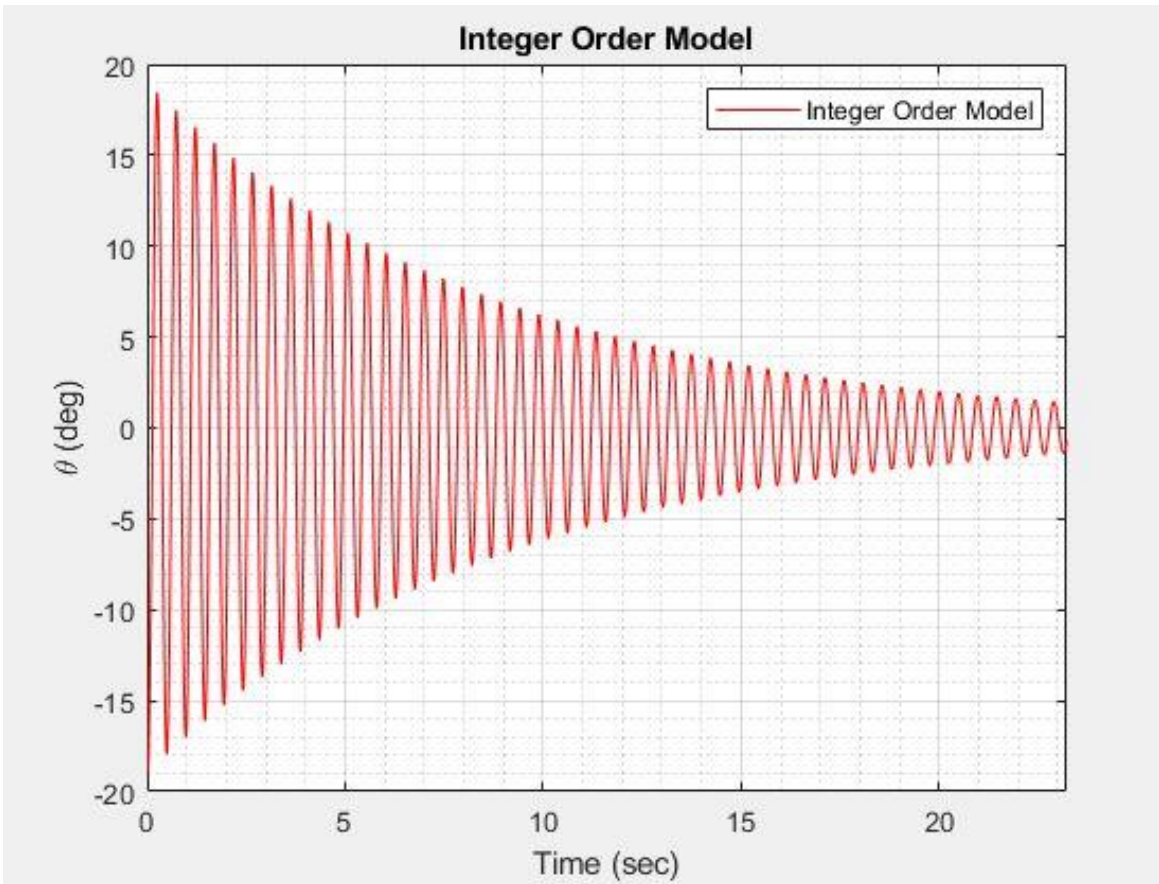


Figure 4.2 Graph of the integer order model approximation.

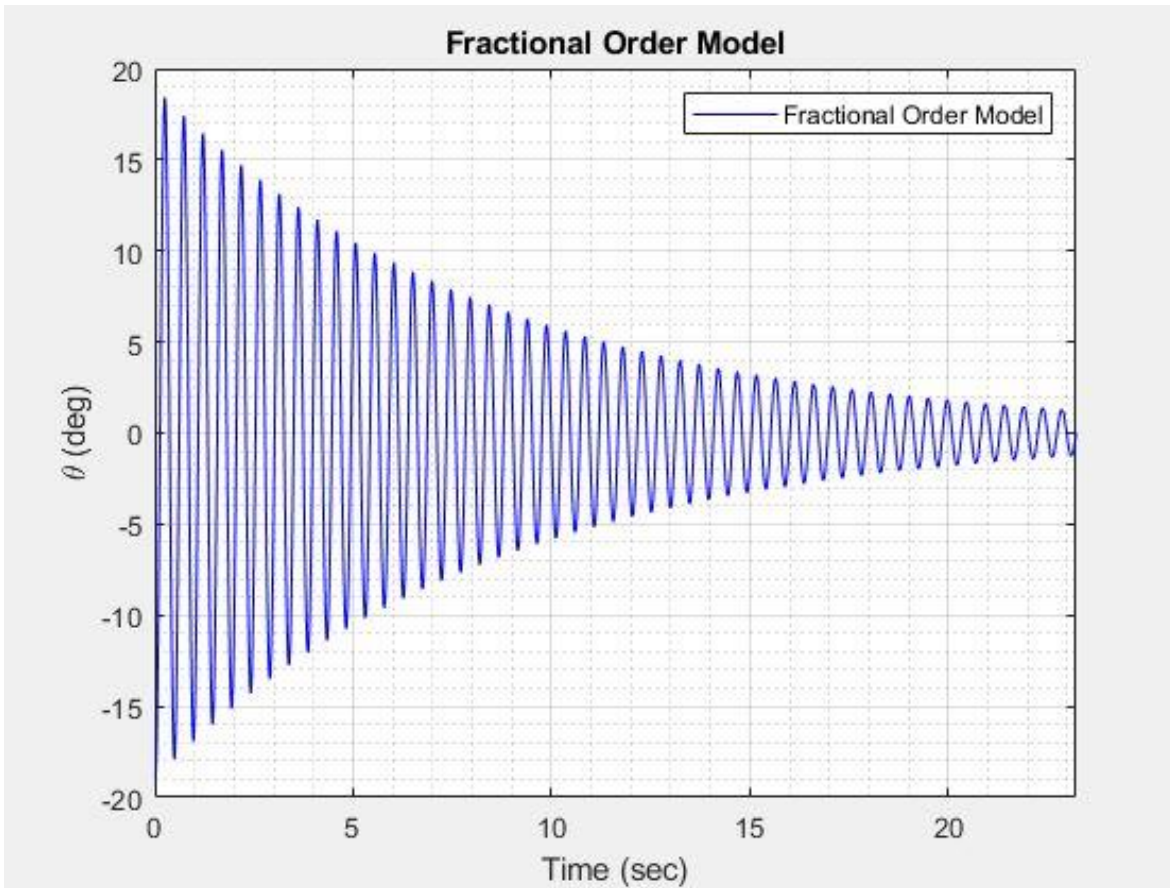


Figure 4.3 Graph of the fractional order model approximation.

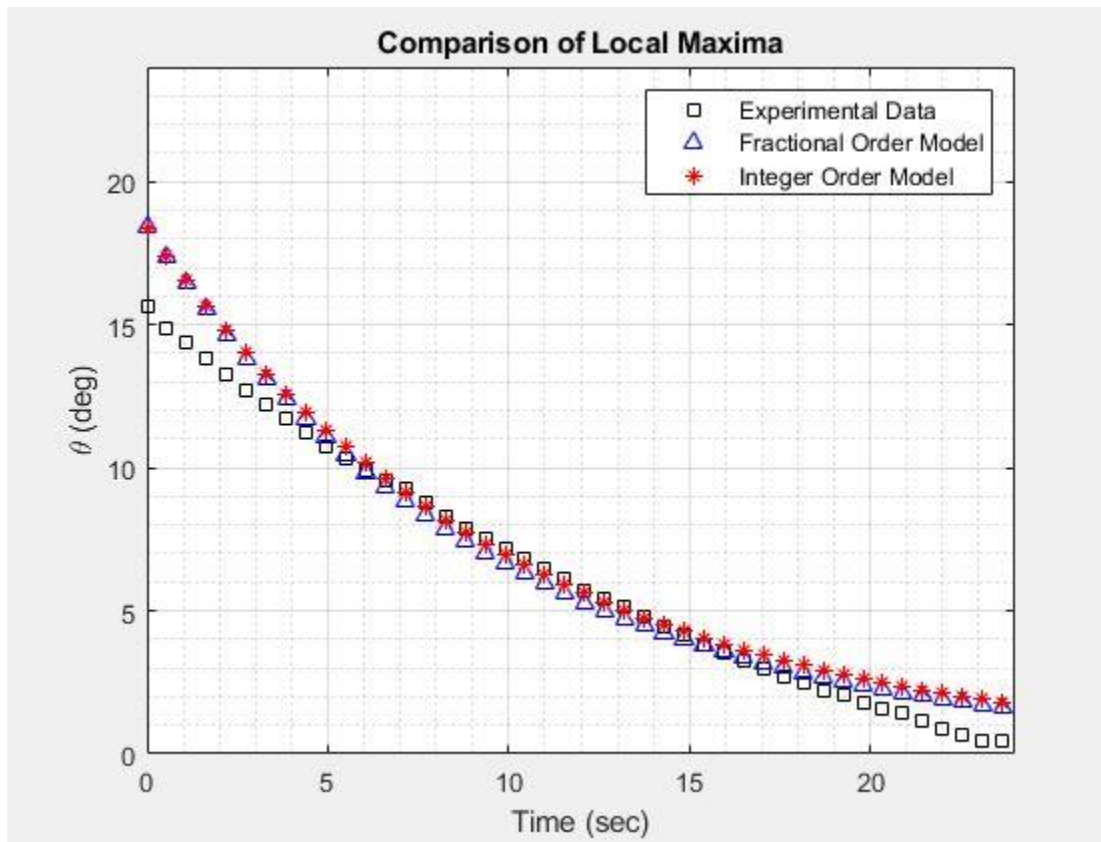


Figure 4.4 Plot for the comparison of local maxima of the experimental data and models.

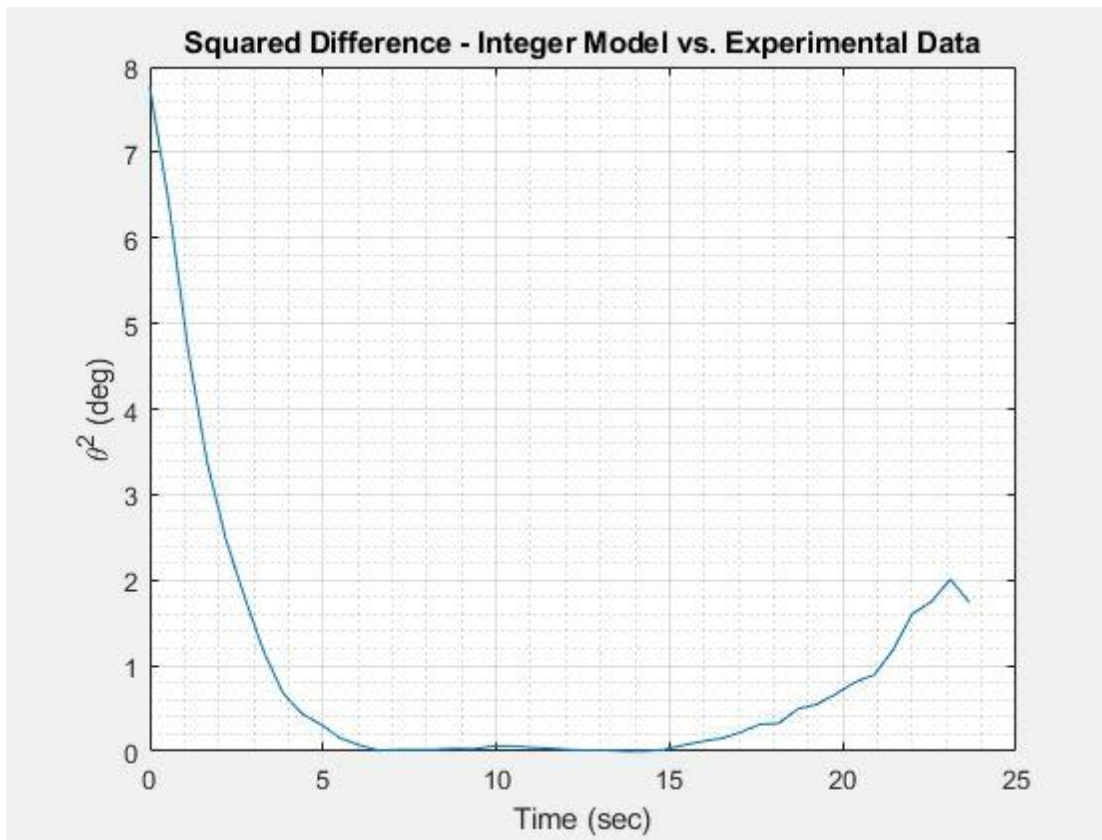


Figure 4.5 Plot for squared difference between integer model and experimental data.

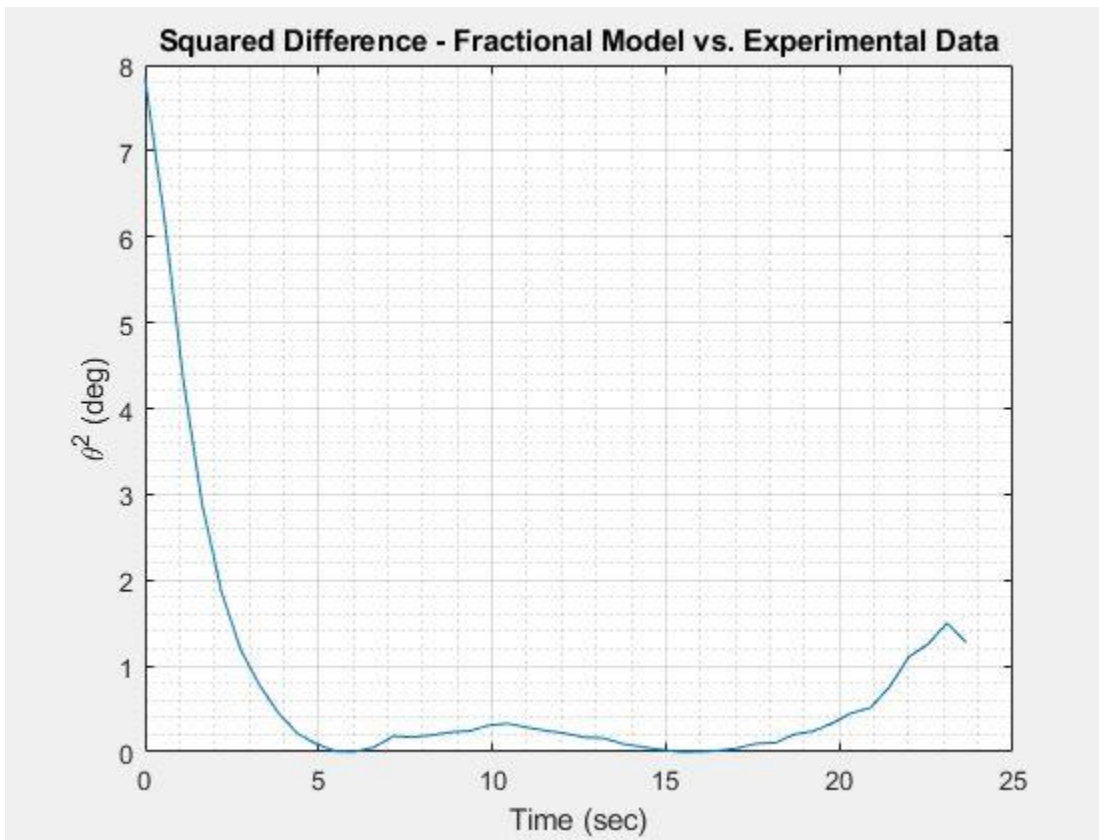


Figure 4.6 Plot for the squared difference between fractional model and experimental data.

CHAPTER 5. SUMMARY, CONCLUSION, AND RECOMMENDATIONS

The fractional order mathematical model approximated the angular position of the oscillating system using the Bagley and Torvik fractional derivative. The experiment validated the application of fractional order calculus to determine the analytical solution for the differential equations governing the physics of the oscillating system. The graphical comparisons between the experimental data and the integer and fractional order models were illustrated in Figures 4.1 through 4.6. The squared difference calculated between the experimental data and the mathematical models is graphically represented by Figure 4.5 and Figure 4.6 and represented by equation 4.1 above. The largest squared difference calculated was 7.77 degrees squared between the integer order model and the experimental data as shown in Figure 4.5. The largest squared difference calculated was 7.849 degrees squared between the fractional order model and the experimental data as shown in Figure 4.6. The largest squared difference occurred at $t = 0$ seconds. The input spin force at $t = 0$ seconds is performed by hand motion and suspected to cause uneven loading resulting in frictional loss. The squared difference between the mathematical models and the experimental data approaches zero from $t = 5$ seconds to $t = 15$ seconds as shown in Figures 4.5 and 4.6. After $t = 15$ seconds, the largest squared difference calculated between the experimental data and the integer and fractional models is 2.00 degrees squared and 1.50 degrees squared, respectively. The fatigue stresses acting on the torsion spring are suspected to cause plastic deformation after 30-40 oscillations and are assumed to be the source of error after $t = 15$ seconds.

The experiment conducted for the mentioned study has improvements to be made for future efforts. Magnetic or pneumatic bearings could be used to further reduce mechanical friction. Angular displacement was limited during the experiment to 20 degrees or less to prevent flexing of the wooden structure. Although the system is assumed to be in free response, the input spin force is performed by hand motion and potentially causes uneven loading resulting in frictional losses. The input spin force should be applied by a known force acting in a known direction at a known angle to minimize error at $t = 0$ seconds. A fully metal support structure with welded joints is recommended to increase the angular displacement in later experiments and minimize the stresses in supporting components such as the set screws, wooden support structure, and the steel nails within the wooden support structure. The experiment conducted in this study used

purified water, but other fluids can be used to observe the differences in the mathematical models by changing fluid density and viscosity.

LIST OF REFERENCES

- Cham, T.S., & Head, M. R. (1969). Turbulent boundary-layer flow on a rotating disk. *Journal of Fluid Mechanics*, 37(1), 129–147. doi: 10.1017/s0022112069000450
- Choudhuri, R., & French, R. M. (2018, May). Experimental Study of Fractional order Behavior in a Dynamic System. Retrieved on 09/23/2019 from <https://docs.lib.purdue.edu/dissertations/AAI10792681>
- Dzieliński, A., Sarwas, G., & Sierociuk, D. (2011). Comparison and validation of integer and fractional order ultracapacitor models. *Advances in Difference Equations*, 2011(1). doi: 10.1186/1687-1847-2011-11
- Escalante-Martínez, J., Gómez-Aguilar, J., Calderón-Ramón, C., Morales-Mendoza, L., Cruz-Orduña, I., & Laguna-Camacho, J. (2016). Experimental Evaluation of Viscous Damping Coefficient in the Fractional Underdamped Oscillator. *Advances in Mechanical Engineering*, 8(4), 168781401664306. doi: 10.1177/1687814016643068
- Garrappa, R., & Popolizio, M. (2018). Computing the Matrix Mittag-Leffler Function with Applications to Fractional Calculus. *Journal of Scientific Computing*, 77(1), 129–153. doi: 10.1007/s10915-018-0699-5
- Howle, V., & Trefethen, L. N. (2001). Eigenvalues and musical instruments. *Journal of Computational and Applied Mathematics*, 135(1), 23–40. doi: 10.1016/s0377-0427(00)00560-4
- Kulish, V., & Lage, J. (2002, September). Application of Fractional Calculus to Fluid Mechanics. Retrieved on 09/24/2019 from https://www.academia.edu/7776802/Application_of_Fractional_Calculus_to_Fluid_Mechanics

- Kleinz, M., & Osler, T. J. (2000). A Childs Garden of Fractional Derivatives. *The College Mathematics Journal*, 31(2), 82. doi: 10.2307/2687575
- Magin, R. L. (2006). *Fractional Calculus in Bioengineering*. Redding, CT: Begell House.
- Podlubny, I. (1999). *Fractional Differential Equations: An Introduction to Fractional Derivatives, Fractional Differential Equations, to Methods of Their Solution and Some of Their Applications*. San Diego: Academic Press, v. 198.
- Rosenthal, A. (1951). The History of Calculus. *The American Mathematical Monthly*, 58(2), 75-86. doi:10.2307/2308368. Date accessed: 11/17/2019.
- Tepljakov, A. (2017). Applications of Fractional order Control. *Fractional order Modeling and Control of Dynamic Systems Springer Theses*, 131–167. doi: 10.1007/978-3-319-52950-9_7
- Torvik, P. J., & Bagley, R. L. (1984). On the Appearance of the Fractional Derivative in the Behavior of Real Materials. *Journal of Applied Mechanics*, 51(2), 294-298. doi:10.1115/1.3167615

APPENDIX A. EXPERIMENTAL DATA

Table 1. Experimental Data.

Time (sec)	θ (Deg)
0.000	0.018
0.017	0.012
0.033	0.014
0.050	0.015
0.067	0.016
0.083	0.018
0.100	0.018
0.117	0.018
0.133	0.019
0.150	0.014
0.167	0.016
0.184	0.015
0.200	0.018
0.217	0.011
0.234	0.016
0.250	0.005
0.267	0.007
0.284	0.010
0.300	0.008
0.317	0.015
0.334	0.013
0.350	0.015
0.367	0.014
0.384	0.015
0.400	0.018
0.417	0.013
0.434	-0.012
0.450	-0.128
0.467	-0.187
0.484	-0.294
0.501	-0.417
0.517	-0.519
0.534	-0.655
0.551	-0.810
0.567	-0.976
0.584	-1.143

0.601	-1.331
0.617	-1.569
0.634	-1.755
0.651	-1.932
0.667	-2.104
0.684	-2.264
0.701	-2.428
0.717	-2.592
0.734	-2.747
0.751	-2.916
0.767	-3.070
0.784	-3.231
0.801	-3.395
0.817	-3.566
0.834	-3.724
0.851	-3.902
0.868	-4.086
0.884	-4.313
0.901	-4.535
0.918	-4.717
0.934	-4.915
0.951	-5.276
0.968	-5.454
0.984	-5.683
1.001	-5.865
1.018	-6.064
1.034	-6.276
1.051	-6.348
1.068	-6.524
1.084	-6.681
1.101	-6.840
1.118	-6.987
1.134	-7.129
1.151	-7.276
1.168	-7.485
1.185	-7.606
1.201	-7.765
1.218	-7.831
1.235	-7.937
1.251	-8.033
1.268	-8.197

1.285	-8.356
1.301	-8.506
1.318	-8.616
1.335	-8.791
1.351	-8.946
1.368	-9.142
1.385	-9.350
1.401	-9.564
1.418	-9.740
1.435	-9.920
1.451	-10.100
1.468	-10.260
1.485	-10.440
1.502	-10.596
1.518	-10.759
1.535	-10.927
1.552	-11.145
1.568	-11.264
1.585	-11.413
1.602	-11.569
1.618	-11.776
1.635	-11.902
1.652	-12.143
1.668	-12.326
1.685	-12.534
1.702	-12.738
1.718	-12.955
1.735	-13.217
1.752	-13.476
1.768	-13.772
1.785	-14.065
1.802	-14.399
1.818	-14.744
1.835	-15.076
1.852	-15.420
1.869	-15.799
1.885	-16.196
1.902	-16.614
1.919	-17.072
1.935	-17.567
1.952	-17.942

1.969	-18.358
1.985	-18.720
2.002	-18.913
2.019	-18.780
2.035	-18.325
2.052	-17.566
2.069	-16.300
2.085	-14.684
2.102	-12.568
2.119	-9.757
2.135	-6.922
2.152	-3.615
2.169	-0.228
2.186	3.231
2.202	6.481
2.219	9.409
2.236	11.908
2.252	13.813
2.269	15.114
2.286	15.606
2.302	15.501
2.319	14.443
2.336	12.945
2.352	10.655
2.369	8.065
2.386	4.967
2.402	1.711
2.419	-1.694
2.436	-5.073
2.452	-8.088
2.469	-10.731
2.486	-12.828
2.503	-14.369
2.519	-15.188
2.536	-15.297
2.553	-14.697
2.569	-13.379
2.586	-11.460
2.603	-8.972
2.619	-6.134
2.636	-2.940

2.653	0.268
2.669	3.644
2.686	6.794
2.703	9.428
2.719	11.876
2.736	13.437
2.753	14.626
2.769	14.890
2.786	14.703
2.803	13.573
2.819	12.054
2.836	9.729
2.853	7.114
2.870	4.030
2.886	0.883
2.903	-2.346
2.920	-5.595
2.936	-8.367
2.953	-10.852
2.970	-12.727
2.986	-14.064
3.003	-14.707
3.020	-14.678
3.036	-13.965
3.053	-12.553
3.070	-10.664
3.086	-8.137
3.103	-5.324
3.120	-2.212
3.136	0.919
3.153	4.144
3.170	7.100
3.187	9.565
3.203	11.769
3.220	13.206
3.237	14.224
3.253	14.361
3.270	13.975
3.287	12.749
3.303	11.099
3.320	8.844

3.337	6.263
3.353	3.313
3.370	0.231
3.387	-2.854
3.403	-5.968
3.420	-8.556
3.437	-10.868
3.453	-12.512
3.470	-13.693
3.487	-14.152
3.504	-14.000
3.520	-13.172
3.537	-11.700
3.554	-9.700
3.570	-7.261
3.587	-4.459
3.604	-1.536
3.620	1.555
3.637	4.580
3.654	7.381
3.670	9.726
3.687	11.698
3.704	13.002
3.720	13.744
3.737	13.827
3.754	13.228
3.770	12.073
3.787	10.314
3.804	8.113
3.820	5.432
3.837	2.648
3.854	-0.375
3.871	-3.329
3.887	-6.242
3.904	-8.677
3.921	-10.799
3.937	-12.343
3.954	-13.337
3.971	-13.653
3.987	-13.342
4.004	-12.378

4.021	-10.882
4.037	-8.880
4.054	-6.496
4.071	-3.669
4.087	-0.865
4.104	2.178
4.121	5.059
4.137	7.595
4.154	9.768
4.171	11.526
4.188	12.732
4.204	13.254
4.221	13.229
4.238	12.516
4.254	11.326
4.271	9.421
4.288	7.309
4.304	4.638
4.321	1.885
4.338	-0.944
4.354	-3.827
4.371	-6.576
4.388	-8.863
4.404	-10.737
4.421	-12.107
4.438	-12.932
4.454	-13.129
4.471	-12.713
4.488	-11.658
4.505	-10.173
4.521	-8.066
4.538	-5.741
4.555	-3.002
4.571	-0.260
4.588	2.569
4.605	5.319
4.621	7.726
4.638	9.744
4.655	11.286
4.671	12.356
4.688	12.717

4.705	12.596
4.721	11.744
4.738	10.524
4.755	8.593
4.771	6.442
4.788	3.885
4.805	1.091
4.821	-1.598
4.838	-4.357
4.855	-6.810
4.872	-9.002
4.888	-10.706
4.905	-11.960
4.922	-12.599
4.938	-12.618
4.955	-12.161
4.972	-11.034
4.988	-9.460
5.005	-7.374
5.022	-5.104
5.038	-2.392
5.055	0.248
5.072	3.016
5.088	5.641
5.105	7.770
5.122	9.747
5.138	11.050
5.155	12.040
5.172	12.202
5.189	12.045
5.205	11.062
5.222	9.747
5.239	7.830
5.255	5.647
5.272	3.163
5.289	0.537
5.305	-2.057
5.322	-4.747
5.339	-7.073
5.355	-9.065
5.372	-10.581

5.389	-11.634
5.405	-12.188
5.422	-12.056
5.439	-11.503
5.455	-10.288
5.472	-8.700
5.489	-6.597
5.506	-4.318
5.522	-1.720
5.539	0.866
5.556	3.460
5.572	5.954
5.589	7.925
5.606	9.757
5.622	10.867
5.639	11.707
5.656	11.732
5.672	11.454
5.689	10.399
5.706	9.078
5.722	7.111
5.739	4.985
5.756	2.532
5.772	-0.005
5.789	-2.524
5.806	-5.037
5.822	-7.137
5.839	-9.023
5.856	-10.395
5.873	-11.329
5.889	-11.703
5.906	-11.511
5.923	-10.815
5.939	-9.561
5.956	-7.926
5.973	-5.909
5.989	-3.657
6.006	-1.181
6.023	1.349
6.039	3.822
6.056	6.132

6.073	7.934
6.089	9.600
6.106	10.571
6.123	11.240
6.139	11.193
6.156	10.740
6.173	9.673
6.190	8.269
6.206	6.367
6.223	4.291
6.240	1.891
6.256	-0.566
6.273	-2.976
6.290	-5.334
6.306	-7.301
6.323	-9.006
6.340	-10.221
6.356	-10.992
6.373	-11.216
6.390	-10.955
6.406	-10.195
6.423	-8.912
6.440	-7.236
6.456	-5.258
6.473	-3.008
6.490	-0.617
6.507	1.757
6.523	4.144
6.540	6.265
6.557	7.972
6.573	9.427
6.590	10.255
6.607	10.749
6.623	10.606
6.640	10.070
6.657	8.972
6.673	7.472
6.690	5.624
6.707	3.508
6.723	1.218
6.740	-1.154

6.757	-3.484
6.773	-5.661
6.790	-7.505
6.807	-9.062
6.823	-10.154
6.840	-10.763
6.857	-10.864
6.874	-10.516
6.890	-9.602
6.907	-8.313
6.924	-6.605
6.940	-4.649
6.957	-2.405
6.974	-0.170
6.990	2.152
7.007	4.405
7.024	6.312
7.040	7.929
7.057	9.219
7.074	9.996
7.090	10.337
7.107	10.179
7.124	9.495
7.140	8.416
7.157	6.895
7.174	5.068
7.191	3.007
7.207	0.777
7.224	-1.468
7.241	-3.709
7.257	-5.742
7.274	-7.423
7.291	-8.803
7.307	-9.725
7.324	-10.210
7.341	-10.211
7.357	-9.739
7.374	-8.795
7.391	-7.464
7.407	-5.767
7.424	-3.829

7.441	-1.695
7.457	0.445
7.474	2.675
7.491	4.799
7.508	6.555
7.524	8.073
7.541	9.091
7.558	9.798
7.574	9.895
7.591	9.711
7.608	8.902
7.624	7.845
7.641	6.264
7.658	4.483
7.674	2.461
7.691	0.327
7.708	-1.781
7.724	-3.896
7.741	-5.735
7.758	-7.354
7.774	-8.555
7.791	-9.389
7.808	-9.726
7.824	-9.676
7.841	-9.103
7.858	-8.090
7.875	-6.763
7.891	-5.104
7.908	-3.202
7.925	-1.086
7.941	0.940
7.958	3.063
7.975	5.040
7.991	6.587
8.008	8.022
8.025	8.894
8.041	9.537
8.058	9.546
8.075	9.240
8.091	8.381
8.108	7.267

8.125	5.659
8.141	3.960
8.158	1.960
8.175	-0.090
8.192	-2.142
8.208	-4.152
8.225	-5.813
8.242	-7.279
8.258	-8.365
8.275	-9.064
8.292	-9.287
8.308	-9.088
8.325	-8.470
8.342	-7.419
8.358	-6.093
8.375	-4.396
8.392	-2.562
8.408	-0.566
8.425	1.402
8.442	3.437
8.458	5.280
8.475	6.724
8.492	8.034
8.509	8.734
8.525	9.243
8.542	9.099
8.559	8.762
8.575	7.816
8.592	6.604
8.609	4.990
8.625	3.313
8.642	1.374
8.659	-0.617
8.675	-2.544
8.692	-4.425
8.709	-5.965
8.725	-7.314
8.742	-8.241
8.759	-8.826
8.775	-8.915
8.792	-8.674

8.809	-8.000
8.825	-6.897
8.842	-5.585
8.859	-3.969
8.876	-2.159
8.892	-0.249
8.909	1.682
8.926	3.597
8.942	5.277
8.959	6.599
8.976	7.762
8.992	8.369
9.009	8.757
9.026	8.573
9.042	8.111
9.059	7.134
9.076	5.960
9.092	4.423
9.109	2.716
9.126	0.889
9.142	-1.051
9.159	-2.862
9.176	-4.625
9.193	-6.062
9.209	-7.273
9.226	-8.081
9.243	-8.560
9.259	-8.590
9.276	-8.242
9.293	-7.496
9.309	-6.430
9.326	-5.014
9.343	-3.399
9.359	-1.643
9.376	0.149
9.393	2.004
9.409	3.796
9.426	5.302
9.443	6.512
9.459	7.555
9.476	8.070

9.493	8.299
9.510	8.080
9.526	7.551
9.543	6.589
9.560	5.363
9.576	3.826
9.593	2.185
9.610	0.410
9.626	-1.403
9.643	-3.167
9.660	-4.743
9.676	-6.100
9.693	-7.179
9.710	-7.872
9.726	-8.239
9.743	-8.175
9.760	-7.758
9.776	-6.959
9.793	-5.829
9.810	-4.498
9.826	-2.880
9.843	-1.217
9.860	0.555
9.877	2.301
9.893	3.981
9.910	5.322
9.927	6.465
9.943	7.285
9.960	7.760
9.977	7.891
9.993	7.606
10.010	6.955
10.027	5.987
10.043	4.739
10.060	3.328
10.077	1.696
10.093	-0.008
10.110	-1.725
10.127	-3.357
10.143	-4.816
10.160	-6.030

10.177	-6.950
10.194	-7.568
10.210	-7.777
10.227	-7.681
10.244	-7.139
10.260	-6.315
10.277	-5.223
10.294	-3.831
10.310	-2.351
10.327	-0.704
10.344	0.918
10.360	2.621
10.377	4.156
10.394	5.368
10.410	6.432
10.427	7.093
10.444	7.491
10.460	7.439
10.477	7.139
10.494	6.440
10.511	5.479
10.527	4.178
10.544	2.825
10.561	1.217
10.577	-0.415
10.594	-2.035
10.611	-3.583
10.627	-4.847
10.644	-5.967
10.661	-6.777
10.677	-7.292
10.694	-7.419
10.711	-7.260
10.727	-6.673
10.744	-5.822
10.761	-4.690
10.777	-3.349
10.794	-1.883
10.811	-0.285
10.827	1.236
10.844	2.831

10.861	4.276
10.878	5.322
10.894	6.300
10.911	6.818
10.928	7.195
10.944	7.047
10.961	6.757
10.978	5.956
10.994	5.017
11.011	3.709
11.028	2.360
11.044	0.869
11.061	-0.716
11.078	-2.226
11.094	-3.685
11.111	-4.839
11.128	-5.855
11.144	-6.497
11.161	-6.940
11.178	-6.960
11.195	-6.732
11.211	-6.136
11.228	-5.289
11.245	-4.170
11.261	-2.857
11.278	-1.426
11.295	0.075
11.311	1.539
11.328	3.028
11.345	4.320
11.361	5.295
11.378	6.153
11.395	6.581
11.411	6.850
11.428	6.600
11.445	6.269
11.461	5.441
11.478	4.504
11.495	3.193
11.512	1.882
11.528	0.431

11.545	-1.068
11.562	-2.494
11.578	-3.838
11.595	-4.857
11.612	-5.794
11.628	-6.333
11.645	-6.647
11.662	-6.625
11.678	-6.297
11.695	-5.667
11.712	-4.798
11.728	-3.699
11.745	-2.390
11.762	-1.060
11.778	0.392
11.795	1.765
11.812	3.171
11.828	4.314
11.845	5.201
11.862	5.955
11.879	6.281
11.895	6.461
11.912	6.137
11.929	5.748
11.945	4.880
11.962	3.980
11.979	2.701
11.995	1.410
12.012	0.068
12.029	-1.387
12.045	-2.707
12.062	-3.888
12.079	-4.853
12.095	-5.639
12.112	-6.127
12.129	-6.320
12.145	-6.274
12.162	-5.831
12.179	-5.219
12.196	-4.305
12.212	-3.219

12.229	-1.999
12.246	-0.686
12.262	0.660
12.279	2.017
12.296	3.301
12.312	4.312
12.329	5.140
12.346	5.782
12.362	6.013
12.379	6.100
12.396	5.782
12.412	5.303
12.429	4.476
12.446	3.513
12.462	2.334
12.479	1.060
12.496	-0.215
12.513	-1.568
12.529	-2.824
12.546	-3.867
12.563	-4.799
12.579	-5.461
12.596	-5.863
12.613	-5.967
12.629	-5.815
12.646	-5.357
12.663	-4.691
12.679	-3.812
12.696	-2.727
12.713	-1.552
12.729	-0.280
12.746	0.994
12.763	2.233
12.779	3.413
12.796	4.303
12.813	5.041
12.829	5.512
12.846	5.737
12.863	5.704
12.880	5.375
12.896	4.798

12.913	3.996
12.930	3.020
12.946	1.871
12.963	0.694
12.980	-0.525
12.996	-1.773
13.013	-2.970
13.030	-3.899
13.046	-4.732
13.063	-5.279
13.080	-5.628
13.096	-5.628
13.113	-5.471
13.130	-4.984
13.146	-4.329
13.163	-3.396
13.180	-2.368
13.197	-1.232
13.213	0.005
13.230	1.176
13.247	2.353
13.263	3.404
13.280	4.166
13.297	4.860
13.313	5.196
13.330	5.399
13.347	5.266
13.363	4.951
13.380	4.320
13.397	3.526
13.413	2.563
13.430	1.508
13.447	0.366
13.463	-0.777
13.480	-1.920
13.497	-3.029
13.514	-3.854
13.530	-4.621
13.547	-5.028
13.564	-5.313
13.580	-5.290

13.597	-5.006
13.614	-4.506
13.630	-3.842
13.647	-2.950
13.664	-1.938
13.680	-0.888
13.697	0.255
13.714	1.371
13.730	2.511
13.747	3.377
13.764	4.129
13.780	4.720
13.797	4.959
13.814	5.120
13.830	4.861
13.847	4.510
13.864	3.848
13.881	3.135
13.897	2.162
13.914	1.184
13.931	0.073
13.947	-1.055
13.964	-2.089
13.981	-3.085
13.997	-3.821
14.014	-4.487
14.031	-4.823
14.047	-5.009
14.064	-4.947
14.081	-4.661
14.097	-4.156
14.114	-3.415
14.131	-2.545
14.147	-1.563
14.164	-0.567
14.181	0.537
14.198	1.543
14.214	2.587
14.231	3.360
14.248	3.983
14.264	4.533

14.281	4.645
14.298	4.779
14.314	4.476
14.331	4.150
14.348	3.481
14.364	2.710
14.381	1.836
14.398	0.787
14.414	-0.242
14.431	-1.239
14.448	-2.214
14.464	-3.143
14.481	-3.813
14.498	-4.342
14.515	-4.654
14.531	-4.758
14.548	-4.655
14.565	-4.327
14.581	-3.809
14.598	-3.066
14.615	-2.233
14.631	-1.273
14.648	-0.300
14.665	0.707
14.681	1.688
14.698	2.646
14.715	3.316
14.731	3.871
14.748	4.298
14.765	4.453
14.781	4.465
14.798	4.157
14.815	3.726
14.831	3.091
14.848	2.319
14.865	1.453
14.882	0.526
14.898	-0.421
14.915	-1.397
14.932	-2.353
14.948	-3.092

14.965	-3.685
14.982	-4.126
14.998	-4.356
15.015	-4.394
15.032	-4.205
15.048	-3.843
15.065	-3.321
15.082	-2.626
15.098	-1.867
15.115	-0.940
15.132	-0.038
15.148	0.885
15.165	1.824
15.182	2.658
15.199	3.216
15.215	3.726
15.232	4.018
15.249	4.143
15.265	4.013
15.282	3.719
15.299	3.315
15.315	2.671
15.332	1.921
15.349	1.058
15.365	0.142
15.382	-0.740
15.399	-1.591
15.415	-2.405
15.432	-3.069
15.449	-3.575
15.465	-3.957
15.482	-4.168
15.499	-4.136
15.516	-3.963
15.532	-3.537
15.549	-3.023
15.566	-2.354
15.582	-1.562
15.599	-0.743
15.616	0.107
15.632	0.944

15.649	1.826
15.666	2.527
15.682	3.031
15.699	3.507
15.716	3.679
15.732	3.790
15.749	3.649
15.766	3.345
15.782	2.855
15.799	2.276
15.816	1.517
15.832	0.730
15.849	-0.093
15.866	-0.913
15.883	-1.726
15.899	-2.510
15.916	-3.080
15.933	-3.524
15.949	-3.824
15.966	-3.967
15.983	-3.861
15.999	-3.654
16.016	-3.245
16.033	-2.696
16.049	-2.046
16.066	-1.269
16.083	-0.519
16.099	0.302
16.116	1.049
16.133	1.848
16.149	2.465
16.166	2.915
16.183	3.326
16.200	3.443
16.216	3.507
16.233	3.306
16.250	3.008
16.266	2.518
16.283	1.914
16.300	1.229
16.316	0.480

16.333	-0.264
16.350	-1.061
16.366	-1.753
16.383	-2.422
16.400	-2.925
16.416	-3.344
16.433	-3.530
16.450	-3.578
16.466	-3.472
16.483	-3.202
16.500	-2.835
16.517	-2.286
16.533	-1.661
16.550	-0.934
16.567	-0.249
16.583	0.544
16.600	1.229
16.617	1.958
16.633	2.498
16.650	2.859
16.667	3.178
16.683	3.210
16.700	3.249
16.717	2.995
16.733	2.685
16.750	2.190
16.767	1.655
16.783	1.018
16.800	0.314
16.817	-0.422
16.833	-1.103
16.850	-1.756
16.867	-2.375
16.884	-2.773
16.900	-3.119
16.917	-3.263
16.934	-3.299
16.950	-3.164
16.967	-2.867
16.984	-2.508
17.000	-1.976

17.017	-1.402
17.034	-0.740
17.050	-0.069
17.067	0.590
17.084	1.251
17.100	1.876
17.117	2.329
17.134	2.668
17.150	2.942
17.167	2.975
17.184	2.946
17.201	2.679
17.217	2.366
17.234	1.876
17.251	1.366
17.267	0.734
17.284	0.075
17.301	-0.577
17.317	-1.235
17.334	-1.812
17.351	-2.348
17.367	-2.698
17.384	-3.003
17.401	-3.101
17.417	-3.038
17.434	-2.874
17.451	-2.556
17.467	-2.203
17.484	-1.704
17.501	-1.093
17.518	-0.522
17.534	0.083
17.551	0.717
17.568	1.338
17.584	1.868
17.601	2.205
17.618	2.510
17.634	2.697
17.651	2.676
17.668	2.654
17.684	2.354

17.701	2.027
17.718	1.554
17.734	1.046
17.751	0.518
17.768	-0.091
17.784	-0.721
17.801	-1.279
17.818	-1.757
17.834	-2.206
17.851	-2.533
17.868	-2.708
17.885	-2.806
17.901	-2.725
17.918	-2.544
17.935	-2.223
17.951	-1.875
17.968	-1.391
17.985	-0.887
18.001	-0.295
18.018	0.250
18.035	0.811
18.051	1.377
18.068	1.851
18.085	2.145
18.101	2.367
18.118	2.512
18.135	2.493
18.151	2.360
18.168	2.138
18.185	1.843
18.202	1.379
18.218	0.890
18.235	0.389
18.252	-0.176
18.268	-0.741
18.285	-1.256
18.302	-1.708
18.318	-2.056
18.335	-2.326
18.352	-2.460
18.368	-2.534

18.385	-2.396
18.402	-2.222
18.418	-1.895
18.435	-1.553
18.452	-1.082
18.468	-0.593
18.485	-0.097
18.502	0.404
18.519	0.885
18.535	1.384
18.552	1.751
18.569	2.010
18.585	2.195
18.602	2.221
18.619	2.192
18.635	2.051
18.652	1.816
18.669	1.523
18.685	1.082
18.702	0.595
18.719	0.199
18.735	-0.320
18.752	-0.788
18.769	-1.238
18.785	-1.651
18.802	-1.904
18.819	-2.153
18.835	-2.216
18.852	-2.236
18.869	-2.084
18.886	-1.901
18.902	-1.589
18.919	-1.240
18.936	-0.843
18.952	-0.415
18.969	0.067
18.986	0.535
19.002	0.912
19.019	1.376
19.036	1.683
19.052	1.869

19.069	2.034
19.086	2.029
19.102	2.005
19.119	1.845
19.136	1.563
19.152	1.292
19.169	0.891
19.186	0.438
19.203	0.055
19.219	-0.413
19.236	-0.830
19.253	-1.230
19.269	-1.563
19.286	-1.750
19.303	-1.922
19.319	-2.012
19.336	-2.012
19.353	-1.884
19.369	-1.705
19.386	-1.397
19.403	-1.072
19.419	-0.708
19.436	-0.286
19.453	0.090
19.469	0.539
19.486	0.889
19.503	1.238
19.520	1.505
19.536	1.681
19.553	1.815
19.570	1.731
19.586	1.694
19.603	1.537
19.620	1.281
19.636	1.007
19.653	0.683
19.670	0.263
19.686	-0.093
19.703	-0.448
19.720	-0.873
19.736	-1.209

19.753	-1.445
19.770	-1.597
19.786	-1.725
19.803	-1.726
19.820	-1.719
19.836	-1.565
19.853	-1.391
19.870	-1.095
19.887	-0.815
19.903	-0.456
19.920	-0.095
19.937	0.246
19.953	0.574
19.970	0.904
19.987	1.217
20.003	1.373
20.020	1.527
20.037	1.594
20.053	1.538
20.070	1.466
20.087	1.340
20.103	1.071
20.120	0.854
20.137	0.547
20.153	0.223
20.170	-0.095
20.187	-0.431
20.204	-0.757
20.220	-1.040
20.237	-1.244
20.254	-1.388
20.270	-1.439
20.287	-1.431
20.304	-1.390
20.320	-1.240
20.337	-1.069
20.354	-0.838
20.370	-0.577
20.387	-0.266
20.404	0.049
20.420	0.364

20.437	0.652
20.454	0.924
20.470	1.191
20.487	1.313
20.504	1.380
20.521	1.421
20.537	1.376
20.554	1.269
20.571	1.110
20.587	0.891
20.604	0.655
20.621	0.405
20.637	0.093
20.654	-0.185
20.671	-0.445
20.687	-0.734
20.704	-0.917
20.721	-1.083
20.737	-1.223
20.754	-1.238
20.771	-1.234
20.787	-1.158
20.804	-1.009
20.821	-0.837
20.837	-0.661
20.854	-0.389
20.871	-0.175
20.888	0.134
20.904	0.343
20.921	0.589
20.938	0.807
20.954	0.997
20.971	1.116
20.988	1.131
21.004	1.149
21.021	1.110
21.038	0.979
21.054	0.892
21.071	0.654
21.088	0.475
21.104	0.288

21.121	0.014
21.138	-0.200
21.154	-0.432
21.171	-0.656
21.188	-0.833
21.205	-0.965
21.221	-1.003
21.238	-1.011
21.255	-0.993
21.271	-0.917
21.288	-0.826
21.305	-0.667
21.321	-0.503
21.338	-0.327
21.355	-0.104
21.371	0.097
21.388	0.304
21.405	0.482
21.421	0.652
21.438	0.796
21.455	0.819
21.471	0.849
21.488	0.824
21.505	0.795
21.522	0.685
21.538	0.589
21.555	0.442
21.572	0.287
21.588	0.119
21.605	-0.084
21.622	-0.240
21.638	-0.379
21.655	-0.520
21.672	-0.668
21.688	-0.712
21.705	-0.800
21.722	-0.809
21.738	-0.752
21.755	-0.682
21.772	-0.584
21.788	-0.472

21.805	-0.334
21.822	-0.179
21.838	-0.015
21.855	0.148
21.872	0.308
21.889	0.460
21.905	0.582
21.922	0.663
21.939	0.682
21.955	0.667
21.972	0.643
21.989	0.618
22.005	0.523
22.022	0.448
22.039	0.310
22.055	0.158
22.072	0.006
22.089	-0.143
22.105	-0.238
22.122	-0.366
22.139	-0.485
22.155	-0.522
22.172	-0.571
22.189	-0.571
22.206	-0.526
22.222	-0.507
22.239	-0.466
22.256	-0.358
22.272	-0.296
22.289	-0.188
22.306	-0.049
22.322	0.053
22.339	0.139
22.356	0.268
22.372	0.328
22.389	0.449
22.406	0.478
22.422	0.476
22.439	0.482
22.456	0.467
22.472	0.442

22.489	0.341
22.506	0.306
22.523	0.169
22.539	0.124
22.556	0.000
22.573	-0.070
22.589	-0.165
22.606	-0.204
22.623	-0.264
22.639	-0.339
22.656	-0.342
22.673	-0.342
22.689	-0.339
22.706	-0.312
22.723	-0.310
22.739	-0.203
22.756	-0.171
22.773	-0.052
22.789	-0.015
22.806	0.057
22.823	0.125
22.839	0.148
22.856	0.181
22.873	0.229
22.890	0.294
22.906	0.300
22.923	0.299
22.940	0.281
22.956	0.197
22.973	0.165
22.990	0.139
23.006	0.089
23.023	0.081
23.040	0.009
23.056	-0.022
23.073	-0.027
23.090	-0.051
23.106	-0.050
23.123	-0.043
23.140	-0.072
23.156	-0.033

23.173	-0.020
23.190	-0.006
23.207	0.000
23.223	0.001

APPENDIX B. MATLAB CODE

```
%%%%%%%%%%%%%%%%%%%%%%%%%%%%%%%%%%%%%%%%%%%%%%%%%%%%%%%%%%%%%%%%%%%%%%%%
% THIS CODE SOLVES FOR THE INTEGER AND FRACTIONAL ORDER %
% MODELS FOR THE PROPOSED EXPERIMENT. %
%%%%%%%%%%%%%%%%%%%%%%%%%%%%%%%%%%%%%%%%%%%%%%%%%%%%%%%%%%%%%%%%%%%%%%%%

clear all
close all
clc

%
%importing experimental data collected from Tracker Software
data = importdata('7_32_in_rod_wet_trial_01_txt.txt');

%
%creating array to store experimental data imported from text file
[n_size,~] = size(data);
time_exp = zeros(n_size,1);
theta_exp = zeros(n_size,1);
time_exp = data(:,1);
theta_exp = data(:,2);

ti = 0;
t_offset = 2.002;

tf = 25;
dt = 0.01;
T = time_exp(end);
N = round(T/dt);

%
%COMPUTING INTEGER ORDER MODEL
%

%
%integer order model parameters
A_int = 0.0625;
B_int = 0.12;
C_int = 10.6;

%
%initial conditions
theta_int(1) = -18.913;
theta_int(2) = -18.913;

%
%for loop computes integer order model for angular position
for i = 2:N
    theta_int(i+1) = -dt^2/A_int*(B_int/dt*(theta_int(i) - theta_int(i-1)) +
C_int*theta_int(i-1)) + 2*theta_int(i) - theta_int(i-1);
end
time_int = dt*(1:length(theta_int));
```

```

%
%COMPUTING FRACTIONAL ORDER MODEL
%
%constant coefficients for fractional model
A_frac = 0.0721;
B_frac = 0.0017;
C_frac = 10.6;

%
%initial conditions
theta_frac(1) = -18.9132;
theta_frac(2) = -18.9132;

omega = 0;

%
%alpha-th derivative for fractional model
alpha = 1.5;

%
%for loop computes fractional order model for angular position
for m = 2:N

    %computing omega for fractional order model
    for j = 1:m
        omega = (-1)^j*gamma(alpha+1)/(gamma(j+1)*gamma(alpha-j+1));
    end
    theta_frac(m+1) = (dt^2*(-C_frac*theta_frac(m)) +
A_frac*(2*theta_frac(m)-theta_frac(m-1)) -
B_frac*sqrt(dt)*omega*theta_frac(m-1))/(A_frac + B_frac*sqrt(dt));

end

time_frac = dt*(1:length(theta_frac));

%
%GENERATING PLOTS
%
%
%plot for experimental data
figure(1)
plot((time_exp((time_exp>t_offset))-
t_offset),theta_exp((time_exp>t_offset)), 'k')
hold on
grid on
grid minor

```

```

axis([0 (T-t_offset) -20 20])
xlabel('Time (sec)')
ylabel('\theta (deg)')
legend('Experimental Data')
title('Experimental Data')

%
%plot for integer model
figure(2)
plot(time_int,theta_int, 'r')
grid on
grid minor
axis([0 T -20 20])
xlabel('Time (sec)')
ylabel('\theta (deg)')
legend('Integer Order Model')
title('Integer Order Model')

%
%plot for fractional model
figure(3)
plot(time_frac,theta_frac, 'b')
grid on
grid minor
axis([0 T -20 20])
xlabel('Time (sec)')
ylabel('\theta (deg)')
legend('Fractional Order Model')
title('Fractional Order Model')

%
%plot for experimental data and integer model
figure(4)
plot(time_int,theta_int, 'r')
grid on
hold on
grid minor
plot((time_exp((time_exp>t_offset))-
t_offset),theta_exp((time_exp>t_offset)), 'k')
axis([0 T -20 20])
xlabel('Time (sec)')
ylabel('\theta (deg)')
legend('Integer Order Model', 'Experimental Data')
title('Experimental Data vs. Integer Order Model')

%
%plot for experimental data and fractional model
figure(5)
plot(time_frac,theta_frac, 'b')
grid on
hold on
grid minor
plot((time_exp((time_exp>t_offset))-
t_offset),theta_exp((time_exp>t_offset)), 'k')
hold on
grid on

```

```

grid minor
axis([0 T -20 20])
ylabel('\theta (deg)')
xlabel('Time (sec)')
legend('Fractional Order Model', 'Experimental Data')
title('Experimental Data vs. Fractional Order Model')

%
%plot for experimental data, integer, and fractional model
figure(6)
plot(time_int,theta_int, 'r')
hold on
plot(time_frac,theta_frac, 'b')
grid on
hold on
grid minor
plot((time_exp((time_exp>t_offset))-
t_offset),theta_exp((time_exp>t_offset)), 'k')
axis([0 T -20 20])
xlabel('Time (sec)')
ylabel('\theta (deg)')
legend('Integer Order Model', 'Fractional Order Model', 'Experimental Data')
title('Comparison of Experimental Data to Integer and Fractional Models')

%time offset included to compensate for initial spin force to respect the
%assumption of free response system
data_cropped = xlsread('7_32_in_rod_wet_trial_0001.xlsx');
[nn_size,~] = size(data_cropped);
time_exp_cropped = zeros(nn_size,1);
theta_exp_cropped = zeros(nn_size,1);
time_exp_cropped = data_cropped(:,1);
theta_exp_cropped = data_cropped(:,2);
theta_exp_cropped_0 = theta_exp_cropped(1:end-1);

%
%Fractional model error
theta_interp_frac = interp1(time_frac, theta_frac, time_exp_cropped);

theta_interp_frac_0 = theta_interp_frac(2:end);

% %
% %Integer model error
theta_interp_int = interp1(time_int, theta_int, time_exp_cropped);
%
theta_interp_int_0 = theta_interp_int(2:end);

%
%comparing int vs frac models
figure(7)
plot(time_int,theta_int, 'r')
hold on
plot(time_frac,theta_frac, 'b')
grid on
hold on
grid minor
axis([0 T -20 20])

```

```

xlabel('Time (sec)')
ylabel('\theta^2 (deg)')
title('Integer Order Model vs. Fractional Order Model')
legend('Integer Order Model', 'Fractional Order Model')

error_frac_int = (theta_frac - theta_int).^2;

theta_exp_pks = findpeaks(theta_exp_cropped);

time_exp_pks = 0:0.525:24;
time_pks = 0:0.55:24;
[mm_size,~] = size(theta_exp_pks);
theta_exp_pks_0 = zeros(mm_size,1);
theta_exp_pks_00 = theta_exp_pks(1:end-2);

theta_frac_pks = findpeaks(theta_interp_frac_0);

theta_int_pks = findpeaks(theta_interp_int_0);

figure(8)
plot(time_pks, theta_exp_pks_00, 'ks')
xlim([0 T])
hold on
grid on
grid minor
plot(time_pks, theta_frac_pks, 'b^')
plot(time_pks, theta_int_pks, 'r*')
xlabel('Time (sec)')
ylabel('\theta (deg)')
legend('Experimental Data', 'Fractional Order Model', 'Integer Order Model')
title('Comparison of Local Maxima')

sq_error_int_frac = transpose((theta_frac_pks - theta_int_pks).^2);
sq_error_exp_int = (theta_exp_pks_00 - theta_int_pks).^2;
sq_error_exp_frac = (theta_exp_pks_00 - theta_frac_pks).^2;

figure(9)
plot(time_pks, sq_error_exp_int)
grid on
grid minor
xlim([0 T])
title('Squared Difference - Integer Model vs. Experimental Data')
xlabel('Time (sec)')
ylabel('\theta^2 (deg)')

figure(10)
plot(time_pks, sq_error_exp_frac)
grid on
grid minor
xlim([0 T])
title('Squared Difference - Fractional Model vs. Experimental Data')
xlabel('Time (sec)')
ylabel('\theta^2 (deg)')

```

```
figure(11)
plot(time_pks, sq_error_int_frac)
grid on
grid minor
xlim([0 T])
title('Squared Difference - Fractional Model vs. Integer Model')
xlabel('Time (sec)')
ylabel('\theta^2 (deg)')
```

APPENDIX C. LIST OF EQUATIONS

$$f(x) = e^{px} \quad (2.1)$$

$$\begin{aligned} f^1(x) &= D^1 e^{px} = p^1 * e^{px} \\ f^2(x) &= D^2 e^{px} = p^2 * e^{px} \\ f^3(x) &= D^3 e^{px} = p^3 * e^{px} \end{aligned} \quad (2.2)$$

$$f^n(x) = D^n e^{px} = p^n * e^{px} \quad (2.3)$$

$$f^a(x) = D^a e^{px} = p^a * e^{px} \quad (2.4)$$

$$f^{\frac{1}{2}}(x) = D^{\frac{1}{2}} e^{px} = \sqrt{p} * e^{px} \quad (2.5)$$

$$e^{jx} = \cos(x) + j * \sin(x) \quad (2.6)$$

$$D^n x^p = \frac{p(p-1)(p-2)\dots(p-n+1)(p-n)(p-n-1)\dots 1}{(p-n)(p-n-1)\dots 1} x^{p-n} = \frac{p!}{(p-n)!} x^{p-n} \quad (2.8)$$

$$\Gamma(x) = \int_0^{\infty} e^{-t} t^{x-1} dt \quad (2.9)$$

$$\Gamma(x + 1) = x\Gamma(x) \quad (2.10)$$

$$D^a x^p = \frac{\Gamma(p+1)}{\Gamma(p-a+1)} x^{p-a} \quad (2.11)$$

$$f(x) = \sum_{n=0}^{\infty} a_n x^n \quad (2.12)$$

$$D^a f(x) = \sum_{n=0}^{\infty} a_n D^a x^n = \sum_{n=0}^{\infty} a_n \frac{\Gamma(n+1)}{\Gamma(n-a+1)} x^{n-a} \quad (2.13)$$

$$D^{-1}f(x) = \int_0^x f(t)dt \quad (2.14)$$

$$D^{-2}f(x) = \int_0^x \int_0^{t_2} f(t_1) dt_1 dt_2 \quad (2.15)$$

$$D^{-2}f(x) = \int_0^x \int_{t_1}^x f(t_1) dt_2 dt_1 \quad (2.16)$$

$$D^{-2}f(x) = \int_0^x f(t)(x-t)dt \quad (2.17)$$

$$D^{-3}f(x) = \frac{1}{2} \int_0^x f(t)(x-t)^2 dt \quad (2.18)$$

$$D^{-4}f(x) = \frac{1}{2*3} \int_0^x f(t)(x-t)^3 dt \quad (2.19)$$

$$D^{-n}f(x) = \frac{1}{(n-1)!} \int_0^x f(t)(x-t)^{n-1} dt \quad (2.20)$$

$${}_b D_x^a f(x) = \frac{1}{\Gamma(-a)} \int_b^x \frac{f(t) dt}{(x-t)^{a+1}} \quad (2.21)$$

$$D^a e^x = \sum_{n=0}^{\infty} \frac{1}{n!} x^n = \sum_{n=0}^{\infty} \frac{x^{n-a}}{\Gamma(n-a+1)} \quad (2.22)$$

$${}_b D_x^{-1} e^{ax} = \int_b^x e^{ax} dx = \frac{1}{a} e^{ax} - \frac{1}{a} e^{ab} \quad (2.23)$$

$${}_{-\infty} D_x^a e^{ax} = a^a e^{ax} \quad (2.24)$$

$${}_{-\infty} D_x^a f(x) = \frac{1}{\Gamma(-a)} \int_b^x \frac{f(t) dt}{(x-t)^{a+1}} \quad (2.25)$$

$$m \frac{d^2 x(t)}{dt^2} + c \frac{dx(t)}{dt} + kx(t) = f(t) \quad (2.26)$$

$$m \frac{d^2 x(t)}{dt^2} + c \frac{dx(t)}{dt} + kx(t) = 0 \quad (2.27)$$

$$(\lambda^2 m + \lambda c + k)Ae^{\lambda t} = 0 \Rightarrow \lambda^2 m + \lambda c + k = 0 \quad (2.28)$$

$$\lambda_{1,2} = (-\zeta \pm \sqrt{\zeta^2 - 1}) \sqrt{\frac{k}{m}} \quad (2.29)$$

$$\zeta = \frac{c}{2\sqrt{km}} \quad (2.30)$$

$$\lambda_{1,2} = -\zeta \omega_n \pm i \omega_d \quad (2.31)$$

$$\text{where } \omega_n = \sqrt{\frac{k}{m}} \text{ and } \omega_d = \omega_n \sqrt{1 - \zeta^2}$$

$$l_* = \frac{v}{v_\tau} = \frac{v}{\Omega_z r} \sqrt{\frac{2}{c_f}} = Re^{-2} r \sqrt{\frac{2}{c_f}} \quad (2.32)$$

$$\begin{aligned} \rho \left(\frac{dv_r}{dt} + v_r \frac{dv_r}{dr} + v_\theta \frac{dv_r}{d\theta} - \frac{v_\theta^2}{r} + v_z \frac{dv_r}{dz} \right) = \\ \rho g_r - \frac{dP}{dr} + \mu \left(\frac{d}{dr} \left(\frac{1}{r} * \frac{d}{dr} (rv_r) \right) + \frac{1}{r^2} * \frac{d^2 v_r}{d\theta^2} - \frac{2}{r^2} * \frac{dv_r}{d\theta} + \frac{d^2 v_r}{dz^2} \right) \end{aligned} \quad (2.33)$$

$$\begin{aligned} \rho \left(\frac{dv_\theta}{dt} + v_r \frac{dv_\theta}{dr} + \frac{v_\theta}{r} * \frac{dv_\theta}{d\theta} + \frac{v_r v_\theta}{r} + v_z \frac{dv_\theta}{dz} \right) = \\ \rho g_\theta - \frac{1}{r} * \frac{dP}{d\theta} + \mu \left(\frac{d}{dr} \left(\frac{1}{r} * \frac{d}{dr} (rv_\theta) \right) + \frac{1}{r^2} * \frac{d^2 v_\theta}{d\theta^2} - \frac{2}{r^2} * \frac{dv_\theta}{d\theta} + \frac{d^2 v_\theta}{dz^2} \right) \end{aligned} \quad (2.34)$$

$$\begin{aligned} \rho \left(\frac{dv_z}{dt} + v_r \frac{dv_z}{dr} + \frac{v_\theta}{r} * \frac{dv_z}{d\theta} + v_z \frac{dv_z}{dz} \right) = \\ \rho g_z - \frac{dP}{dz} + \mu \left(\frac{1}{r} * \frac{d}{dr} \left(r \frac{dv_z}{dr} \right) + \frac{1}{r^2} * \frac{d^2 v_z}{d\theta^2} + \frac{d^2 v_z}{dz^2} \right) \end{aligned} \quad (2.35)$$

$$\frac{1}{r} * \frac{d}{dr} (rv_r) + \frac{1}{r} * \frac{dv_\theta}{d\theta} + \frac{dv_z}{dz} = 0 \quad (2.36)$$

$$\tau_\theta = -\mu \left[2 \left(\frac{1}{r} * \frac{dv_\theta}{d\theta} + \frac{v_r}{r} \right) - \frac{2}{3} \left(\frac{1}{r} * \frac{d}{dr} (rv_r) + \frac{1}{r} * \frac{v_\theta}{d\theta} + \frac{dv_z}{dz} \right) \right] \quad (2.37)$$

$$m \frac{d^2 x(t)}{dt^2} + kx(t) + 2A\sqrt{\rho\mu} \frac{d^{\frac{3}{2}} x(t)}{dt^{\frac{3}{2}}} = f(t) \quad (2.38)$$

$$a {}_0 D_t^\beta y(t) + b {}_0 D_t^a y(t) + c y(t) = f(t) \quad (2.39)$$

$$y(t) = \int_0^t G_3(t-\tau) f(\tau) d\tau \quad (2.40)$$

where $G_3 = \frac{1}{A} \sum_{k=0}^{\infty} \frac{(-1)^k}{k!} \left(\frac{c}{A}\right)^k t^{2k+1} E_{\frac{1}{2}, 2+\frac{3k}{2}}^k \left(-\frac{B}{A} \sqrt{t}\right)$, $E_{\lambda, \mu}^k = \frac{d^k}{dy^k} E_{\lambda, \mu}(y) = \sum_{j=0}^{\infty} \frac{(j+k)! y^j}{j! \Gamma(\lambda j + \lambda k + \mu)}$,

and $k = 0, 1, 2, \dots$

$$I \frac{d^2 \theta}{dt} + C \frac{d\theta}{dt} + K\theta = f(t) \quad (3.1)$$

$$I = \frac{\pi \rho h}{2} (r_{outer}^4 - r_{inner}^4) \quad (3.2)$$

$$K = \frac{G\pi D_{rod}^4}{32L} \quad (3.3)$$

$$\theta = A \sin(\omega t + \phi) e^{-\sigma t} \quad (3.4)$$

$$Ay''(t) + B {}_0 D_t^{3/2} y(t) + Cy(t) = f(t) \quad (3.3)$$

$$A = M, \quad B = 2\sqrt{\mu\rho}, \quad C = K$$

$$Squared\ Difference = (\theta_{calc} - \theta_{exp})^2 \quad (4.1)$$